Supplementary Information for *Population size mediates the contribution of high-rate and large-benefit mutations to parallel evolution*

Martijn F. Schenk, Mark P. Zwart, Sungmin Hwang, Philip Ruelens, Eduard Severing, Joachim Krug and J. Arjan G.M. de Visser

Version: February 11, 2022

This document provides a detailed methods section – including both experimental and bioinformatic methods and analyses – and additional results. Note that the underlying data and scripts for analyses are also organized according to the figures and tables in this supplement for easy access. This includes key datasets such as the spreadsheet with all mutations**.** An index of supplementary tables and figures referenced in the main text is provided. At the start of the document, there is also a table detailing statistical results mentioned in the main text organized per figure (**Supplementary Table 1**). Datasets and code for figures presented in the main manuscript and extended results are available from the publisher, whereas those pertaining to this file are available at Dryad (doi:10.5061/dryad.b2rbnzsh2). For any comments or clarification, please contact Mark P. Zwart (M.Zwart@nioo.knaw.nl).

Table of contents

Table of Additional Statistical Results 4

1. Clonal interference, mutation bias and population size 5

2. Experimental methods and results 8

Competition assays 10
TEM β-lactamase activity 10
Genomic DNA extraction 12
High throughput sequencing 13

3. Genomic analyses 14

Mutation classes 14
Primary analysis with a custom pipeline 14
Primary analysis with CLC Genomics Workbench 14
Combining results from the two analyses 15
Detection of structural variants (SVs) 15
Detection of mutations for population samples 16

4. Identification of mutator clones 17

5. Overview of genomics data 20

6. dN/dS and dI/dS analysis 24

7. Repeatability of genomic changes 25

Methodology 25
Nucleotide-level repeatability results 25

8. Regression analysis of the relative frequency of SVs 31

9. Dynamics of genomic changes 32

Muller plots 32
Repeatability of evolution 32

10. Inference of mutation parameters from Wright-Fisher simulations 35

11. MIC effects of different mutation classes 38

12. Analysis of functional targets and evolutionary trajectories 41

Analysis of evolutionary trajectories 44

13. Analysis of gain-of-function and loss-of-function SNPs 46

Index of Supplementary Tables and Figures

Suppl. Table 1: Table of statistical results 4
Suppl. Table 2: Overview of conditions for experimental treatments 9
Suppl. Table 3: Fitness effects of common TEM deletion and activating mutation G238S 9
Suppl. Table 4: Index of dispersion data for the number of mutations per clone 17
Suppl. Table 5: Common deletions in evolved clones 24
Suppl. Table 6: Common duplications in evolved clones 24
Suppl. Table 7: dN/dS and dI/dS results 25
Suppl. Table 8: Nucleotide-level *H*-indexes 30
Suppl. Table 9: Gene-level *H*-indexes 32
Suppl. Table 10: Comparison of mutations detected in clones and final populations 35
Suppl. Table 11: Inferred mutation rates and selection coefficients 39
Suppl. Table 12: Model selection with the AIC for mutational effect size models 41
Suppl. Table 13: Estimated model parameters for mutational effect size models 42
Suppl. Table 14: Overview of all mutations affecting multiple-hit genes 47
Suppl. Fig. 1: Condition at which mutation and selection bias are balanced 7
Suppl. Fig. 2: Map of the pACTEM plasmid 8
Suppl. Fig. 3: TEM β-lactamase activity measurements 12
Suppl. Fig. 4: Histogram of the frequency of mutations in the chromosome 15
Suppl. Fig. 5: Index of dispersion predictions 19
Suppl. Fig. 6: Mutation frequencies per mutation (SNP, Indel, SV) class for non-mutator clones 20
Suppl. Fig. 7: Total mutation frequencies per clone per treatment 21
Suppl. Fig. 8: Comprehensive overview of mutations for all 112 populations 22
Suppl. Fig. 9: Examples of *H*-index calculation 26
Suppl. Fig. 10: Nucleotide-level pairwise similarity index (*H*-index) 27
Suppl. Fig. 11: Comparison of similarity indices 29
Suppl. Fig. 12: Similarity indexes (*H*-indexes) for time-course meta-population samples 34
Suppl. Fig. 13: Overview of the eight different mutational effect-size models fitted to the MIC data 39

Table of Additional Statistical Results

Supplementary Table 1: Statistical results from tests of data presented in the figures.

Figure	Comparison	Test	Results
2B	SNPs in large vs. small non-mutator populations; chromosome only	MWU[a]	U = 920.5, N = 91, P = 0.076
2B	SVs in large vs. small non-mutator populations	MWU[a]	U = 252, N = 91, P < 0.0001
2B	SVs in large vs. small non-mutator populations; plasmid only	MWU[a]	U = 511, N = 91, P = 0.0149
2B	SVs in large vs. small non-mutator populations; chromosome only	MWU[a]	U = 288.5, N = 91, P < 0.0001
2B	Indels in large vs. small non-mutator populations	MWU[a]	U = 707.5, N = 91, P = 0.794
3B	Nucleotide-level pairwise repeatability in small vs. large non-mutator populations, SNPs only	MWU[a]	U = 13, N = 91, P < 0.0001
3B	Nucleotide-level pairwise repeatability in small vs. large non-mutator populations, SVs only	MWU[a]	U = 1335, N = 91, P < 0.0001
3B	Nucleotide-level pairwise repeatability in small vs. large non-mutator populations, Indels only	MWU[a]	U = 979, N = 91, P = 0.017
3B	Nucleotide-level pairwise repeatability in small vs. large non-mutator populations, SNPs in plasmid only	MWU[a]	U = 300, N = 91, P < 0.0001
3B	Nucleotide-level pairwise repeatability in small vs. large non-mutator populations, SNPs in chromosome only	MWU[a]	U = 271, N = 91, P < 0.0001
3B	Nucleotide-level pairwise repeatability in small vs. large non-mutator populations, SVs in plasmid only	MWU[a]	U = 1054, N = 91, P < 0.001
3B	Nucleotide-level pairwise repeatability in small vs. large non-mutator populations, SVs in chromosome only	MWU[a]	U = 1308, N = 91, P < 0.0001
ED[b] Fig. 4B	Gene-level pairwise repeatability in small vs. large populations, SNPs only	MWU[a]	U = 163, N = 91, P < 0.0001
ED[b] Fig. 4B	Gene-level pairwise repeatability in small vs. large populations, SVs only	MWU[a]	U = 1336, N = 91, P < 0.0001
ED[b] Fig. 4B	Gene-level pairwise repeatability in small vs. large populations, Indels only	MWU[a]	U = 602.5, N = 91, P = 0.199

[a] Mann-Whitney *U* test.

[b] Extended Data Figure

1. Clonal interference, mutation bias and population size

In large asexual populations, simultaneously segregating mutations compete for fixation, a phenomenon generally referred to as clonal interference [1-3]. The competition between beneficial mutations implies that mutations of strong effect fix preferentially, but interference also modifies the fixation of linked mutations that are neutral or weakly deleterious [4, 5].

As a simple scenario that illustrates how the balance between mutation supply and selection changes with population size, we consider two competing beneficial mutations with rates $\mu_1 > \mu_2$ and selection coefficients $s_1 < s_2$ that arise in a monomorphic population. For small populations in the strong selection/weak mutation (SSWM) regime, mutations of type $i = 1,2$ appear at rate $N\mu_i$ and fix with a probability proportional to s_i, where N denotes the population size and the SSWM conditions imply that $N\mu_i \ll 1$ and $Ns_i \gg 1$ [6]. The rate of fixation is therefore proportional to $s_i\mu_i N$, and a straightforward calculation shows that the probability that the mutation 2 of stronger effect fixes first is [7]:

$$P_2 = \frac{\mu_2 s_2}{\mu_1 s_1 + \mu_2 s_2}. \qquad (1)$$

The condition for selection and mutation bias to balance thus reads $s_1\mu_1 = s_2\mu_2$ in the SSWM regime.

An approximate expression for P_2 that remains valid also in the presence of a moderate amount of clonal interference can be obtained by adapting the approach of [8]. The original calculation considered the special case when $\mu_1 = 2\mu_2$ and was based on an estimate of the probability that the mutation of weaker effect fixes before the strong-effect mutation has been established. Generalizing the argument to arbitrary mutation rates and including a heuristic modification that enforces the constraint that $P_2 = \frac{\mu_2}{\mu_1+\mu_2}$ when $s_1 = s_2$, one arrives at the expression:

$$P_2 = 1 - \frac{\mu_1 s_1}{\mu_1 s_1 + \mu_2 s_2} exp\left\{-2N \ln(Ns_1)\mu_2 \left[\frac{s_2}{s_1} - 1\right]\right\}. \qquad (2)$$

This reduces to (1) for small population sizes. Simulations presented in [8] show that this approach is rather accurate at least for the special case $\mu_1 = 2\mu_2$, but more recent work has revealed that it breaks down when the mutation supply rates $N\mu_1$, $N\mu_2$ become large. A formula similar to (2) was

presented by Svensson and Berger [9]. **Fig. 1** in the main text illustrates the dependence of P_2 on the selection bias s_2/s_1 for fixed mutation bias $\mu_1/\mu_2 = 100$ and different population sizes.

To address the regime of strong clonal interference, we refer to a recent study of Gomez et al. [10] on the competition between two simultaneously adapting traits, characterized by different selection coefficients and mutation rates. The traits correspond to the different mutation classes in our system, and the main conclusion that is relevant in our context is that adaptation is dominated by the trait (mutation class) that has the faster rate of adaptation in isolation. Theory reviewed in [3] shows that, to leading order for very large N, the rate of adaptation v for a population subject to a single class of beneficial mutations with selection coefficient s occurring at rate U is given by:

$$v = \frac{s^2 \ln N}{\ln^2 U}. \qquad (3)$$

Note that here $U \ll 1$ denotes the *total* rate of beneficial mutations per individual and generation. In contrast to the SSWM regime where the rate of adaptation is proportional to the mutation supply rate NU, under conditions of strong clonal interference the dependence on U is only logarithmic. As a consequence, moderate differences in selection strength between different mutation classes can be overcome by mutation rate difference only if the mutation bias is extremely strong. Specifically, considering two classes characterized by parameters $U_1 > U_2$ and $s_1 < s_2$, according to Eq. (3), the corresponding rates of adaptation are equal when

$$U_1 = (U_2)^{s_1/s_2}. \qquad (4)$$

For example, to overcome a selection bias $s_2/s_1 = 2$ the mutation rate has to be elevated from U_2 to $U_1 = \sqrt{U_2} \gg U_1$. The relation (4) is illustrated in **Supplementary Fig. 1**.

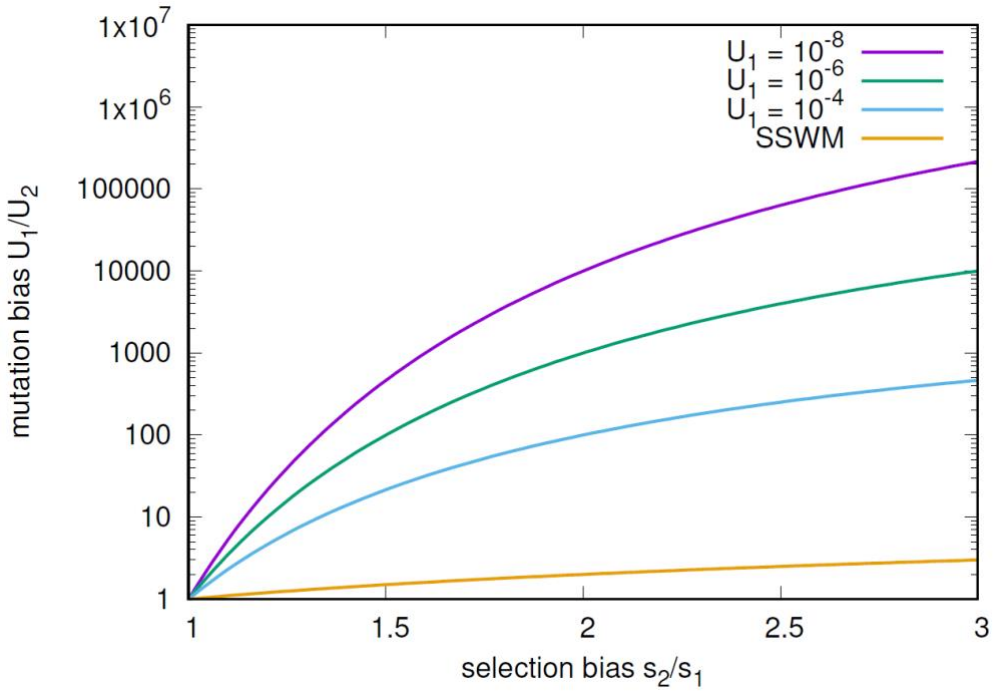

Supplementary Fig. 1. Illustration of condition (4) at which mutation and selection bias are balanced in the regime of very strong clonal interference.

2. Experimental methods and results

Evolution experiment: anciallary details

An overview of the pACTEM plasmid (Genbank MN386081) is given in **Supplementary Fig. 2.** Note the 184-bp repeated regions that flank *bla*$_{TEM1}$ and *lacI*, which are probably responsible for the high rate of deletion events that remove these two genes from the plasmid. A description of the evolution experiment is given in the methods section of the paper, including an overview of the different conditions for small, large and control populations (see **Supplementary Table 2** provided here) and the (increasing) CTX concentrations used for each lineage depending on realized optical density (see **Extended Data Fig. 1**). On three occasions, growth in control wells with medium was detected. In those cases, the entire plate was restarted from the previous day's plate, which was stored at 4˚C. On two occasions the wrong Ara-marker type was detected in a small population, and those populations were restarted from frozen samples from the previous time point. The final cultures were plated out on LB agar with 15 µg/mL tetracycline, and a random clone was selected after overnight growth for subsequent analysis and grown up in 1 mL LB with 15 µg/mL tetracycline to prepare glycerol stocks, except in the case of populations C1-C8, for which no antibiotics were used.

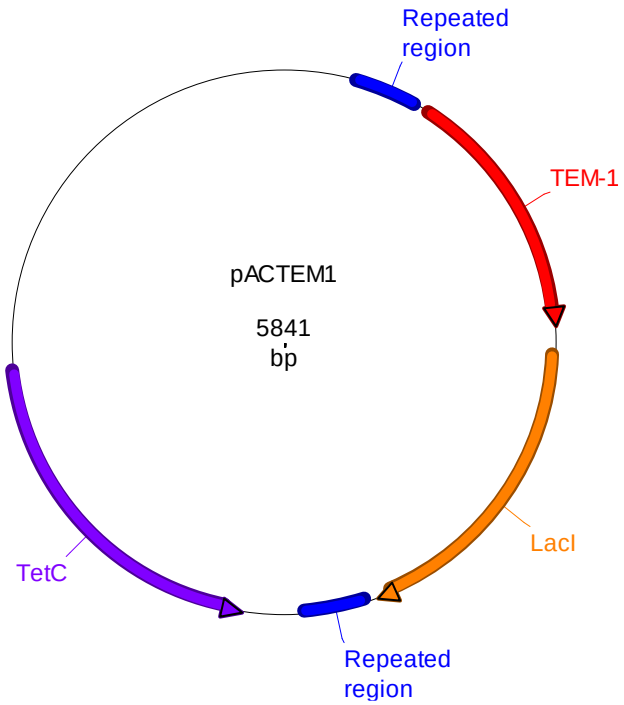

Supplementary Fig. 2: Map of the pACTEM plasmid, with the two blue regions indicating the 184 bp repeated region that probably drives instability of *bla*$_{TEM1}$ and *lacI* genes.

Supplementary Table 2. Overview of conditions for experimental treatments.

Condition	Pop. Numbers[a]	Replicates	Culture volume (mL)	CTX (μg/mL)	IPTG (μM)	Tetracycline (μg/mL)
Small	S1-S72	72	0.2	≥ 0.011	50	15
Large	L1-L24	24	20	≥ 0.011	50	15
No antibiotics	C1-C4	4	20	0	50	0
	C5-C8	4	20	0	0	0
Tetracycline only	C9-C12	4	20	0	50	15
	C13-C16	4	20	0	0	15

[a] Note that in some of the primary analysis files and scripts the populations are numbered consecutive from 1-112. In these cases, 1-24 = L1-L24, 25-96 = S1-S72, 97-112= C1-C16.

Supplementary Table 3. Relative fitness estimates of common TEM deletion and TEM-activating SNP G238S from pairwise competitions against ancestral strain REL606/pACTEM1 for three CTX concentrations.

	TEM deletion			G238S		
mg CTX/L	0	0.01	0.04	0	0.01	0.04
	0.8794	0.8272	1.3131	0.8022	1.1772	1.1961
	0.9328	1.0693	1.0331	0.8740	1.3671	1.7191
	1.1570	0.9719	1.0866	0.6502	0.9620	1.2720
	0.8059	0.8770	0.8948	0.7498	0.9814	1.6123
	0.8668	0.8940	0.8248	0.6856	1.0569	1.2841
	0.9560	0.9389	0.8558	0.6772	1.0220	1.1632
	1.1081	1.6587	1.7013	0.8517	0.8926	1.1109
	1.2035	1.0269	0.9855	0.8426	0.8736	0.8826
	1.2748	0.8306	0.9324	0.5443	0.8073	1.1904
	0.9590	1.2066	0.7801	0.8856	1.0843	1.5536
	0.9732	0.6188	0.7894	0.7701	0.8711	1.1769
	1.1617	0.5935	0.6507	0.6619	1.1114	1.0462
Mean	1.0232	0.9595	0.9873	0.7496	1.0173	1.2673
S.E.M.	0.0437	0.0808	0.0816	0.0308	0.0451	0.0705
t (versus 1)	0.5306	-0.5017	-0.1558	-8.1273	0.3823	3.7896
Two-tailed *P*	0.6062	0.6258	0.8790	5.62E-06*	0.7095	0.0030*

*: significant after serial-Bonferroni correction for multiple testing

Resistance assays

Minimal inhibitory concentration (MIC) assays were performed to determine the resistance of clones and population samples from the final time point, using an assay representative of the experimental conditions. Cultures with a total volume of 200 µL LB were setup, including with 5×10^5 cells/mL, 50 µM IPTG, 15 µg/mL tetracycline, and two-fold serial dilutions of CTX ranging from 512 to 0.25 µg CTX/mL, as well as no CTX. These cultures were grown for 24 h at 37 °C with agitation. Growth was then determined by observing an $OD_{600} > 0.075$, whilst all wells for which $0.04 < OD_{600} < 0.075$ were inspected visually to determine growth. Three biological replicates were performed.

Competition assays

We measured the fitness consequences of two common mutations affecting TEM-1 β-lactamase, i.e. the deletion of ~2 kbp from pACTEM, including bla_{TEM-1} and its repressor *lacI*, and activating SNP G238S, by running pairwise competition assays with constructed mutants against ancestral strain REL606/pACTEM1. To do so, we transformed YFP- and CFP-labelled versions of REL606 with ancestral pACTEM1, pacDEL and pACTEM-G238S plasmids, which were isolated from evolved clones. The YFP- and CFP-labelled REL606 strains were provided by Vaughn Cooper (University of Pittsburgh). Competition assays were performed in 96-well microtiter plates containing 200µl LB supplemented with 50 µM IPTG, 15 µg/mL tetracycline and 0, 0.01 and 0.04 mg CTX/L and were initiated with 1:1,000 dilution from overnight cultures. Each competition was performed with six-fold replication in both fluorescently-marked backgrounds (12-fold replication in total). The frequency of both competitors was estimated prior to inoculation (t=0h) and after incubation (t=24h) at 37°C with shaking (600rpm) by counting YFP and CFP cells in samples of ~10,000 cells using a flow cytometer (MacsQuant Analyzer 10, Miltenyi). Prior to flow cytometry, cells were washed twice and resuspended in 200µl phosphate-buffered saline. Relative fitness was estimated by the ratio of Malthusian parameters [11], and tested for significant deviation from 1 using one-sample *t*-tests with serial-Bonferroni correction for multiple testing (**Supplementary Table 3**, see also **Fig. 4D**). The estimates indicate that the common deletion of TEM and repressor LacI from the plasmid has no fitness consequences, while common activating mutation G238S provides a benefit at CTX concentrations above the starting concentration of 0.011 mg CTX/L (but has a cost below that).

TEM β-lactamase activity

To understand the effects of common chromosomal mutations in genes *pcnB* and *polA* on plasmid copy number, their effect on TEM expression was measured in the large populations. First, each final clone of the large populations was cured of the pACTEM plasmid. This was done by performing two passages with 50 µM IPTG but without any antibiotics, followed by plating of the populations and screening for clones

without tetracycline resistance. The cured clones were then electro-transformed with the ancestral pACTEM1 plasmid. For each final clone, a transformant carrying pACTEM1 was then grown up overnight in LB with 15 µg/mL tetracycline, and subsequently diluted 1,000-fold into LB with 15 µg/mL tetracycline and 50 µM IPTG. After 2 h incubation, the culture was diluted 10-fold into ice-cold phosphate buffered saline (PBS) pH = 7.4 with 2 mg/mL nitrocefin. By pelleting cells (5 min. at 5000 rcf at 4 °C), we could assay the supernatant or the resuspended cells for TEM activity [11]. The plate was then incubated at room temperature (21 °C) for 1 h, and the OD_{490} was measured every minute using a Victor^3 plate reader (Perkin-Elmer). We included a standard curve, based on a stationary phase culture diluted by 4-fold steps in LB. For each time point, we fitted a linear regression to the square root of the expected relative activity (as determined by the dilution of the stationary phase sample) and the observed activity. We then chose the time point with the highest coefficient of determination (r^2) for the standard curve and used only the data from this time point for determining relative TEM activity in the experimental samples using the fitted linear relationship. We then normalized TEM activity by the OD_{600} value of the culture prior to dilution into PBS, to take into account minor differences in cellular density. Three biological replicates were analyzed for each final clone.

As each evolved final clone from the large populations had the ancestral TEM plasmid reintroduced into it, we measured how mutations in *pcnB* and *polA* affected TEM beta-lactamase activity. We found that in most clones, beta-lactamase activity was reduced strongly (**Supplementary Fig. 3**). This reduction of activity was statistically significant for all evolved clones except populations 5 and 18, as determined by a pairwise *t*-test with serial Bonferroni correction. Population 18 is the only of the 24 large populations that does not have mutations in the *pcnB* or *polA* genes, while population 5 harbors a 210-bp deletion in *pcnB*. Given the significant reduction of plasmid copy number in 22 of the 23 populations with mutations in *pcnB* or *polA* (of which many presumably inactivate the gene function), while the only population without these mutations shows no decrease, strongly suggested that mutations in *pcnB* and *polA* result in a reduction of plasmid copy number. As TEM expression is costly, these reduced expression and activity levels are likely to be beneficial for growth in the absence or at low concentrations of CTX.

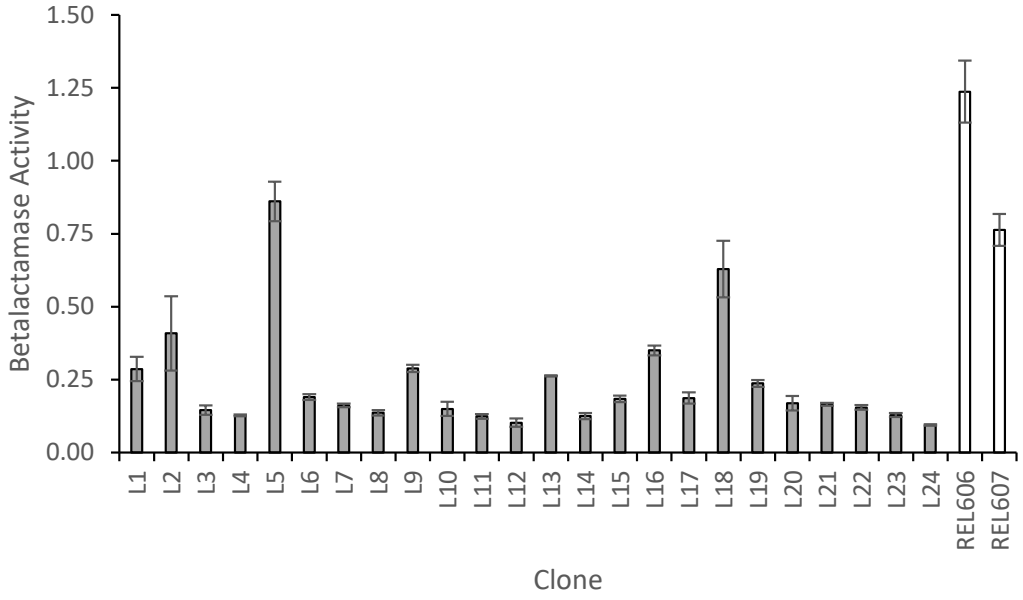

Supplementary Fig. 3: TEM beta-lactamase activity measurements in supernatants from large populations with the ancestral pACTEM plasmid reintroduced. On the x-axis is the clone from the large populations as well as the two ancestors, and on the y-axis is the TEM activity, expressed relative to average of the ancestral REL606/607 clones. For most clones, β-lactamase activity was strongly reduced. All clones had significantly lower activity than both ancestral strains, except L5 and L18. There was a good agreement between measurements on supernatants and cells (r^2 = 0.988).

Genomic DNA extraction

We extracted genomic DNA from the randomly selected clone from the final time point of the small, large and control populations. In addition, from the pool of transformants from which clones were selected to found experimental populations, we sequenced two Ara+ and two Ara- clones. We also sequenced the metagenomes of five small and five large populations from five time points (100, 200, 300, 400 and 500 generations). The populations we sequenced were L1-L5, and S1, S4, S14, S17 and S25. For the small populations, we selected two populations with TEM-activating mutations in the final sequenced clone (S17 and S25) and three random populations. Total genomic DNA was isolated with the Gentra Puregene Yeast/Bacterial DNA extraction kit (Qiagen), following the manufacturer's instructions, including overnight incubation at room temperature with agitation for DNA resuspension. In addition, plasmid DNA was isolated separately with Nucleospin Plasmid DNA kit (Machery-Nagel) and then added to the genomic samples from the same clone/population, to ensure high coverage of the plasmid.

High throughput sequencing

The NexteraXT (Illumina) kit was used for library preparation, and libraries were sequenced by HiSeq 2500 PE150. Library preparation and sequencing were performed by the Cologne Center for Genomics (https://portal.ccg.uni-koeln.de/ccg/index.php). For the 112 clones from the final populations, coverage of the bacterial chromosome was 42.08 ±0.59 (mean ±SEM), and coverage of the plasmid was 524.70 ±66.96. Coverage calculations for the plasmid are based only on those clones with an intact plasmid, and not those with large deletions.

3. Genomic analyses

For detecting mutations in the sequenced clones, two different approaches were used for primary analysis of the Illumina data. First, the data were analyzed using a custom pipeline. Second, the data were analyzed with CLC Genomics Workbench v8.01 (Qiagen Bioinformatics). Data from the two approaches were then compared to validate the identification of genomic changes.

Mutation classes

Note that as in the manuscript proper, we refer to three classes of mutations here: (1) single-nucleotide polymorphisms (SNPs): the substitution on a single nucleotide. (2) Indels: insertion sequence (IS) insertion, and duplication, deletions or inversions with a length <1 Kbp, and (3) structural variants (SVs): duplications, deletions or inversions with a length >1 Kbp.

Primary analysis with a custom pipeline

Raw sequences reads were preprocessed by first removing potential sequencing adaptors using Cutadapt [12] and then trimming low quality regions with Trimmomatic [13]. The cleaned reads were mapped to the genomic sequence using Bowtie2 [14] with default parameters and only those alignments with mapping quality equal or larger than 20 were kept. The alignments were summarized using the mpileup function of the samtools program [15]. Custom python scripts were used to summarize the observed nucleotide frequencies at all genomic positions from the mpileup output.

Primary analysis with CLC Genomics Workbench

The Illumina data were also analyzed with CLC Genomics Workbench. The trim sequences tool was used to trim demultiplexed reads, with default settings except a Phred threshold of 30 (expected error ≤ 1/100). Broken pairs were not discarded because our coverage on the chromosome was not very high. The trimmed reads were mapped to the REL606 genome (Genbank NC_012967.1) and the pACTEM1 sequence (Genbank MN386081), using default settings and with random allocation of ambiguously mapping reads. The basic variant detector was then used to identify mutations, again using default settings. All mutations with a frequency above 0.01 (i.e., 1%) were called. For a small number of regions of the genome where it proved difficult to disentangle mutational events, we extracted the reads from small regions (< 1,000-bp long) and performed *de novo* assembly in CLC Genomics Workbench, using default settings.

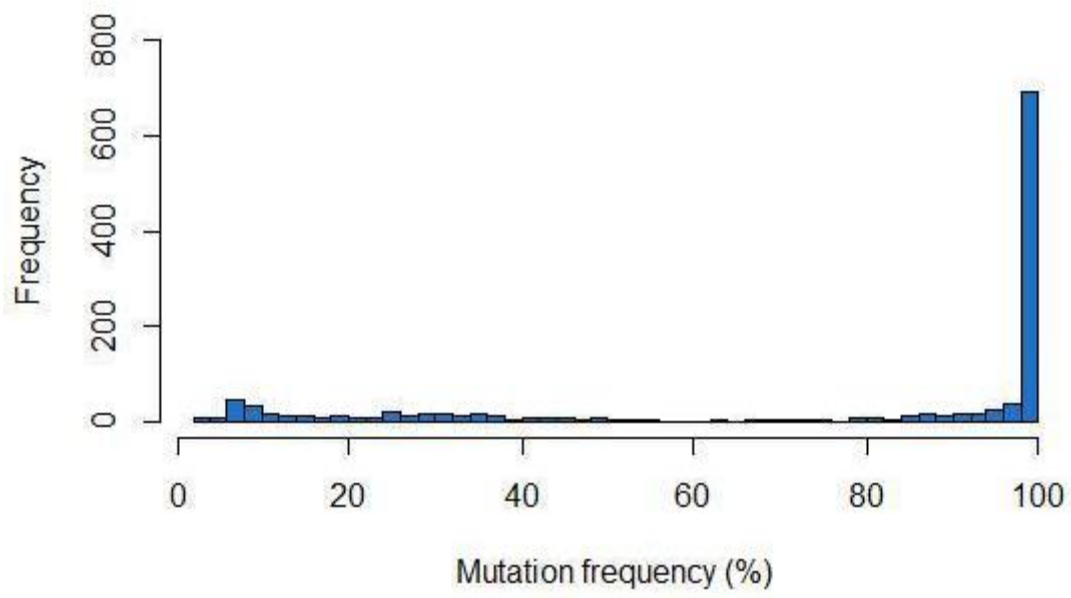

Supplementary Fig. 4: Histogram of the frequency of mutations among reads mapped onto the chromosome for the CLC Genomics Workbench variant calling results of the sequenced clones, prior to manual curation.

Combining results from the two analyses

We compared the variants detected with these two approaches and combined them into a single database. We first eliminated all mutations (i) associated with the ancestral REL607 strain, and (ii) those that were detected in at least one of the four sequenced starting clones. We then flagged mutations that were (i) identified only by one sequence-analysis approach, or (ii) were not categorized as being fixed, or (iii) showed strong strand bias (< 40% or > 60% forward reads). We then manually curated all flagged mutations, discarding those mutations that appeared to be sequencing artifacts. There was generally good agreement between the two approaches, with 97.1% of the mutations accepted (after manual curation) being detected by both methods. The majority of mutations detected were present at high frequency in the reads, as even for the noncurated mutations 66.0 % were present at a frequency > 0.9 (**Supplementary Fig. 4**).

Detection of structural variants (SVs)

During our manual curation of mutational events, we noticed that some larger Indels and SVs (SVs) – in particular events larger than the average read length – had not been detected. We therefore performed additional checks to detect these variants. First, we scanned the sequence alignments for low coverage regions (< 10 reads), and then manually mapped deletions spotted. Second, we plotted the coverage per

base pair and in bins of 100 bp, over the entire genome. This allowed for quick but effective visual inspection, which we combined with *kmeans* algorithms to determine if loci with different levels of coverage were clustered. Upon visual inspection, any regions with higher coverage were then manually checked for duplications. For the analyses of clones, we expect duplications to have fold increases that are whole numbers. When increases in coverage were estimated – by dividing the coverage in the duplicated region by coverage in an immediately upstream region of length > 100,000 bp – only values above 1.75 were considered as real events. We only noticed two events with intermediate coverage levels (1.1 and 1.3 fold), which were disregarded. In addition, when manually curating events called by our custom pipeline and CLC Genomics Workbench, we noticed that some spurious events (e.g., low frequency SNPs) in fact indicated other mutational events, such as the addition of an IS element. Overall, all SVs (213) were detected through the procedures described here. For indels, about a quarter (26.1%, 70/268) were detected through the procedure described here or the general manual curation. Most SNPs were detected automatically, and only a small number was assigned after manual curation (3.6%, 26/706). Finally, we noticed heteroplasmy in eight final clones, as both the intact plasmid and the bla_{TEM1}/*lacI* deletion variant were present. As the frequency of the deletion variant was high (≥ 0.5) in 7/8 cases, we included the bla_{TEM1}/*lacI* deletion in mutations overviews (see also **Supplementary Fig. 9**) and subsequent analyses for these clones. The clone from population S25, next to the the bla_{TEM1}/*lacI* deletion, also includes a large-effect SNP (R241P) in bla_{TEM1} which has fixed in the intact plasmid subpopulation (sequencing coverage > 400). For this clone, we included both ot these mutually exclusive mutations in subsequent analysis: one is at high frequency (bla_{TEM1}/*lacI*) and the other (R241P in bla_{TEM1}) is a known large-effect mutation [16] which is likely in the process of displacing the deletion variant.

Detection of mutations for population samples

For detection of mutations in the population samples from different time points, we used CLC Genomics Workbench for primary sequence data analysis, as described above. Since we expected to find genetic variants at intermediate frequencies, we altered our criteria for accepting mutations. For SNPs and indels, ≥ 5 reads must be present for the mutation to be called, and it must reach a frequency ≥ 0.1 for at least one time point. Similarly, for the ancestral allele to be deemed present, it must also have ≥ 5 reads. Copy number variants must reach a frequency ≤ 0.75 or ≥ 1.25 at one time point to be deemed as real events. There are copies of *lacI* on both the bacterial chromosome and the pACTEM plasmid, which we could not distinguish due to ambiguity with read mapping.

4. Identification of mutator clones

To identify populations that evolved a mutator phenotype, we first looked for mutations in known mutator loci in the clones chosen for sequencing. We found non-synonymous mutations in *mutL* (population L15, S62) and *mutS* (populations L11, L21). We then considered the total number of mutations of all classes that had occurred per clone. Five populations were clearly outliers (**Extended Data Fig. 2**), including the four populations with non-synonymous mutations in *mutL* (L15: 40 mutations; S65: 31 mutations) and *mutS* (L11: 68 mutations; L21: 42 mutations), but also including one other population without mutations in known mutator genes: S62 with 31 mutations. Given the high number of mutations in this clone, we considered this population also a putative mutator. Possibly its high number of mutations was due to unstable genetic changes, such as temporary copy number variation of sequences affecting DNA metabolism and repair.

Next, we considered the index of dispersion I (i.e., the ratio of variance:mean number of mutations) for the mutators and non-mutators separately. Whereas for the non-mutators I was less than the Poisson value $I = 1$, for the mutators it was greater than one (**Supplementary Table 4**). The index of dispersion can take a large value for the mutators, because (i) mutators with inactivating mutations in different mismatch repair systems will have different mutation rates, and (ii) the time when these five different populations evolved a mutator phenotype is likely different, as it depends on the occurence of random mutations. Note that for the non-mutators, $I < 1$ as predicted for conditions under which clonal interference occurs [17]. The index of dispersion can also be considered only for synonymous mutations, which are expected to be mainly neutral (see section 6. dN/dS and dI/dS analysis) and accumulate at a constant rate in lineages. We found $I \sim 1$ for all non-mutator populations as expected, wheras for the mutators I was still above 1 (**Supplementary Table 4**). Although these trends are striking, the number of synonymous mutations observed is small.

Supplementary Table S4: Index of dispersion data for the number of mutations per clone.

Mutations	Clones	Observations	Mean	Variance	Index of dispersion *I*
All	Mutators	5	42.400	230.300	5.43
	Non-mutators Small	21	10.238	7.690	0.75
	Non-mutators Large	70	9.543	3.730	0.39
	Non-mutators	16	5.875	2.383	0.41
Syn. SNPs	Control Mutators	5	6.400	8.300	1.30
	Non-mutators Small	21	0.095	0.090	0.95
	Non-mutators Large	70	0.171	0.173	1.01

Non-mutators Control	16	0.125	0.117	0.93

We considered whether these results for index of dispersion are compatible with the simplest explanation of the data, namely that mutations occurred at random time points. Consider a population that has evolved for *T* generations, and that underwent a switch from a normal state with mutation rate μ_1 to a mutator state with mutation rate $\mu_2 > \mu_1$ at some time *t* with 0 < *t* < *T*. Then the number of mutations accumulated at the endpoint is Poisson distributed with parameter

$$\lambda(t) = \mu_1 t + \mu_2(T - t) = \mu_1 T - (\mu_2 - \mu_1)t \tag{5}$$

For a given λ, the first and second moments of the number of mutations *n* are λ and $\lambda^2 + \lambda$, respectively. Averaging the moments over the (unknown) switching time, the index of dispersion I is found to increase relative to the Poissonian value of 1 according to

$$I = \frac{\mathrm{Var}[n]}{\mathbb{E}[n]} = \frac{\mathbb{E}[\lambda^2] + \mathbb{E}[\lambda] - \mathbb{E}[\lambda]^2}{\mathbb{E}[\lambda]} = 1 + \frac{\mathrm{Var}[\lambda]}{\mathbb{E}[\lambda]} \tag{6}$$

Here $\mathbb{E}[X]$ and $\mathrm{Var}[X]$ denote the expectation value and the variance of the random variable X, respectively. As a simple example, suppose that the switch occurs at a uniformly distributed time between 0 and *T*. Then the evaluation of (6) yields

$$I = 1 + \frac{1}{6}\frac{(\mu_2 - \mu_1)^2 T}{\mu_1 + \mu_2}. \tag{7}$$

For $\mu_2 \gg \mu_1$ this simplifies to $I - 1 \approx \mu_2 T/6$, which is of the order of the total number of mutations accumulated in a mutator strain over *T* generations.

For a somewhat more realistic scenario, we assume that populations switch irreversibly to the mutator state at a constant rate ω per generation. Then the fraction of mutator lines at time *T* is $\varphi(T) = 1 - e^{-\omega T}$, and the evaluation of the moments of the Poisson parameter λ gives the expressions

$$\mathbb{E}[\lambda] = \mu_2 T + \frac{\mu_2 - \mu_1}{\omega}\varphi \tag{8}$$

$$\begin{aligned}\mathbb{E}[\lambda^2] = {} & (1-\varphi)\mu_1^2 T^2 + \varphi\mu_2^2 T^2 - \frac{2T}{\omega}\mu_2(\mu_2 - \mu_1)[\varphi - (1-\varphi)\omega T] \\ & + \frac{2}{\omega^2}(\mu_2 - \mu_1)^2\left[\varphi - (1-\varphi)\left(\omega T + \frac{1}{2}(\omega T)^2\right)\right]\end{aligned} \tag{9}$$

Supplementary Fig. 5 illustrates the resulting behavior of the index of dispersion. For a 32-fold increase in mutation rate for the mutators ($\mu_2/\mu_1 = 32$), consistent with measurements for a constructed *mutS*-defective mutant of the same *E. coli* strain [18], the predicted value of I is compatible with the empirical observation ($I = 5.43$) for the final time point ($\omega T = 10^{-4} \cdot 500 = 0.05$). At long times I reverts to the Poissonian value $I = 1$, because all lines eventually switch to the mutator state, but the decay occurs very slowly (proportional to $1/T$).

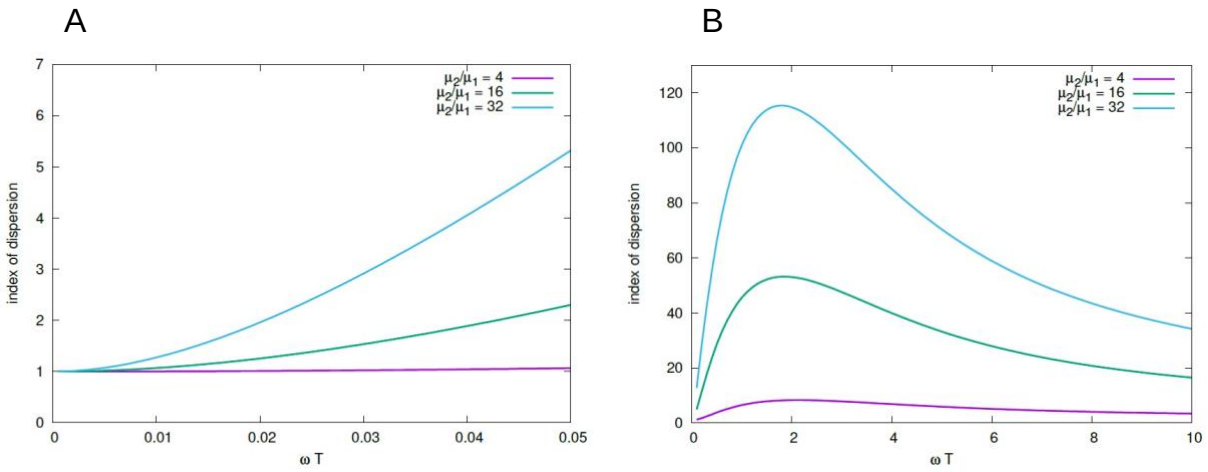

Supplementary Figure 5. Index of dispersion for an ensemble of populations that switch to the mutator state at a constant rate ω. The parameters were chosen to be roughly consistent with the experiment. After $T = 500$ generations about 5% of the lines are mutators, which corresponds to a switching rate of $\omega = 10^{-4}$ per generation. The normal mutation rate is taken to be $\mu_1 = 0.001 = 10 \cdot \omega$, and three different values for the ratio μ_2/μ_1 are shown. Panel A shows I as a function of ωT for the first 500 generations. Panel B illustrates the behavior at long times. For this set of parameters the index of dispersion peaks at time $\omega T = 2$, where about 86% of the lines are mutators.

5. Overview of genomics data

We first considered the number of mutations per mutation class: SNPs are the most common mutations, whereas Indels and SVs occur at lower rates (**Supplementary Fig. 6**; see section 3 for the definition of mutation classes). The large and small populations evolved in increasing CTX concentrations have fixed more mutations per clone than the control populations with only tetracycline or no antibiotics (**Supplementary Fig. 7**). When we consider the distribution of mutations in different classes for different treatments (**Extended Data Fig. 3**), we see clear differences. Clones from large populations have accumulated more SNPs from small populations, whereas clones from large populations have fewer SVs than those from small populations. The tetracycline control has fixed equal numbers of each mutation class, whereas for the no antibiotics control, the pattern is more similar to the large populations: SNPs predominate but overall the numbers of mutations is lower. We can compare the mutation classes in large and small populations, considering whether mutations occur on the bacterial chromosome or the pACTEM plasmid (see **Fig. 2B**). The number of SNPs on the bacterial chromosome is similar for both treatments, whereas there are more SNPs on the plasmid in the large populations. A detailed description of the SVs on the bacterial chromosome is given in **Supplementary Tables 5 and 6**. The number of SVs on the chromosome is higher for the small populations.

We also provide a comprehensive overview of mutations per clone from the evolved populations in **Supplementary Fig. 8**, which includes the control populations.

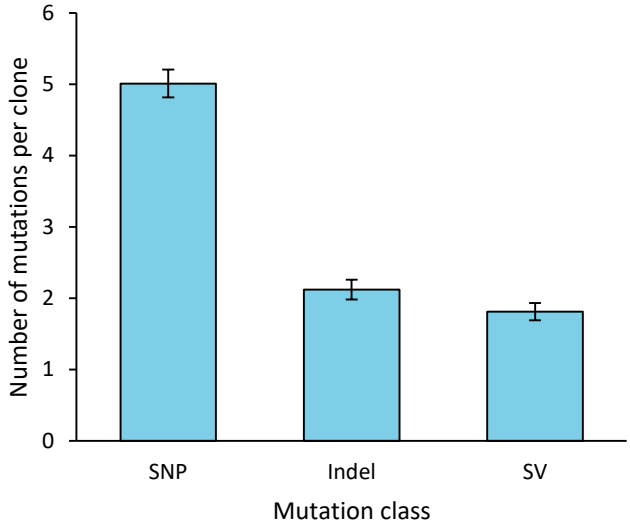

Supplementary Fig. 6: Mutation frequency per mutation class for all 107 non-mutator sequenced clones from evolved populations, with error bars indicating the standard error of the mean. SNP: single nucleotide polymorphism; Indel: indels (<1 kbp) and IS-element insertions; SV: structural variants (> 1 kbp).

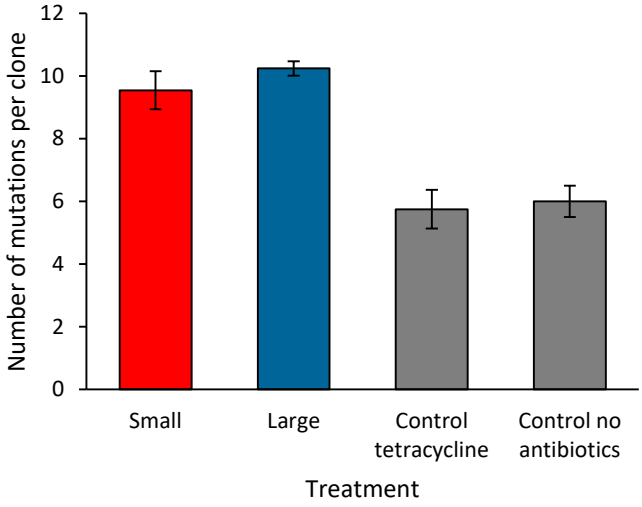

Supplementary Fig. 7: Total mutation frequency per treatment for the 107 non-mutator populations, with error bars indicating the standard error of the mean.

Supplementary Fig. 8 (next page): Comprehensive overview of mutations across chromosome and plasmid per clone from the 112 evolved populations. Control populations are shown at the bottom of the figure, and small and large populations are shown in order of CTX resistance, as indicated to the left in MIC doublings. Small populations have a light blue filling, whereas large have none. The bacterial chromosome is indicated on the center left, and the pACTEM plasmid on the right. Chromosomal positions of rRNA operons and IS elements are shown above. Red and green bars indicate deletions and duplications, respectively, with a size over 1 kbp; yellow bars indicate deletions which have not fixed in the population, which were only observed in the plasmid; downward pointing green triangles and upward pointing red triangles indicate insertions and deletions under 1 kbp, respectively; black circles indicate IS insertions; orange diamonds indicate inversions; dark grey lines are intergenic or synonymous SNPs; black lines are nonsynonymous SNPs; asterisks indicate the five mutator clones.

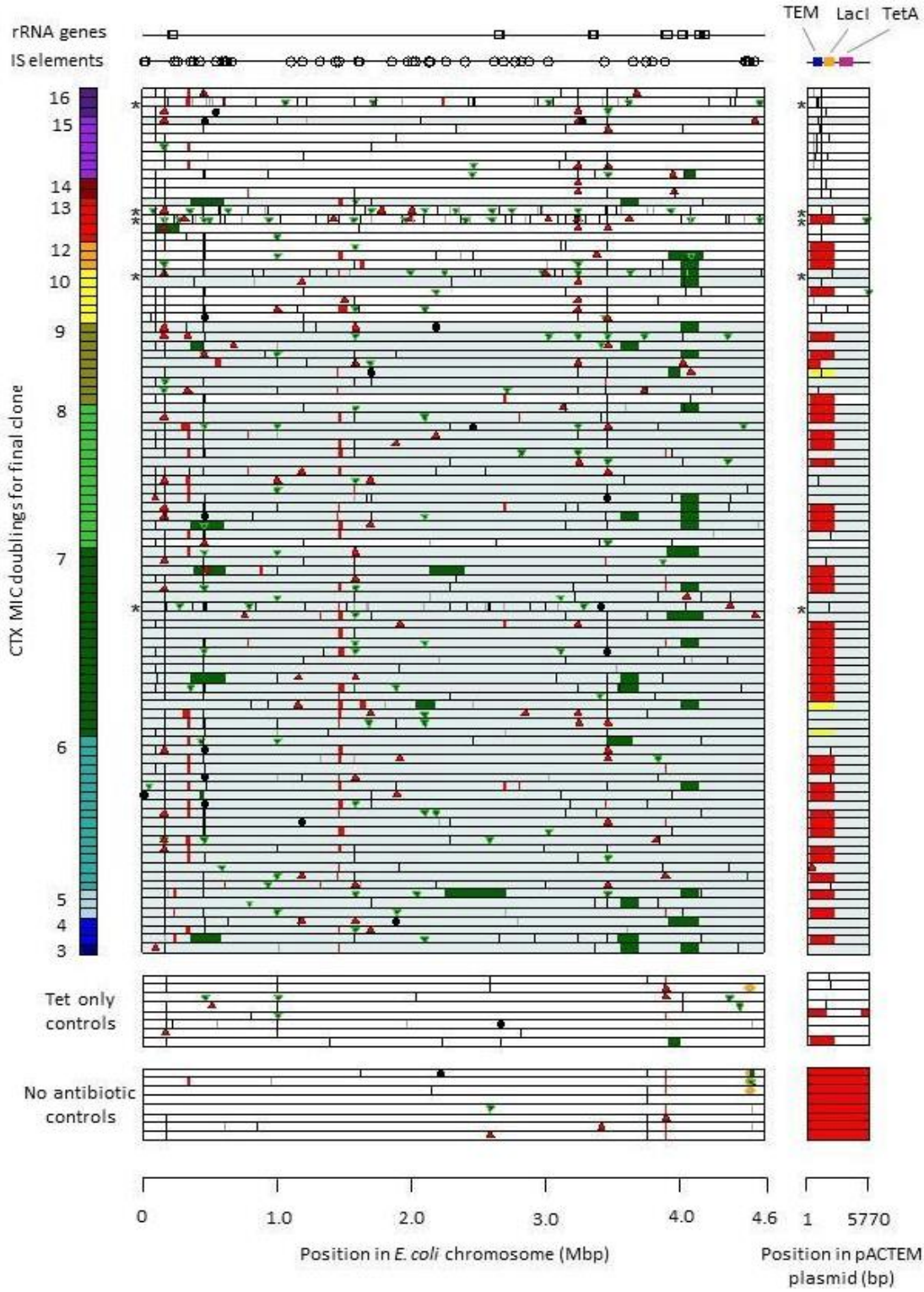
rRNA genes
IS elements
TEM
LacI
TetA
CTX MIC doublings for final clone
16
15
14
13
12
10
9
8
7
6
5
4
3
Tet only controls
No antibiotic controls
0
1.0
2.0
3.0
4.0
4.6
1
5770
Position in E. coli chromosome (Mbp)
Position in pACTEM plasmid (bp)

Supplementary Table 5: Common deletions in evolved clones

Range[a]	Size[b]	Event[c]	Deleted genes	Occurrence			
				S[d]	L[e]	N[f]	T[g]
335,889-353,264	17,365	IS-mediated	*frmAB, lacIZ, mhpABCDEFRT, yaiLO*	20	4	1	0
1,460,931-1,466,876	5,946	IS-mediated	*cybB, hokB, mokB, trg, ydcAIJ,*	35	2	0	0
3,894,997-3,897,893	2,896	IS150-mediated	*rbsACD*	7	0	6	2

[a] The region affected that is shared by these deletions, [b] The size of she shared region denoted by range, [c] Type of event associated with the deletion. [d] Small populations, [e] Large populations, [f] No antibiotics control populations, [g] Tetracycline only control populations.

Supplementary Table 6: Common duplications in evolved clones

Range[a]	Size[b]	Duplicated genes	S[c]	L[d]	N[e]	T[f]
429,491-457,290	28,429	*acrAB, amtB, lon, cof, hha, hupB, glnK, mdlA, maa, ppiD, tesB, ybaABCEJOVWXYZ*	7	0	0	0
3,651,100-3,652,225	1,125	*insJ, insK-4*	9	1	0	0
4,047,731-4,130,407[g]	82,676	*cdh, cpxAPR, csqR, cytR, dtd, eptC, fdhDE, fdoGHI, fief, fpr, frvABRX, frwBCD, fsaB, ftsN, gldA, glpFKX, hslUV, katG, kdgT, menA, metBFJL, pfkA, pflCD, priA, ptsA, rraA, rhaABDMSRT, rpmE, sbp, sodA, tpiA, uspD, yihRSTUVXY, yiiEFGMQRSX, yijEFO, zapB, ECB_03786, ECB_03822*	19	3	0	1

[a] The region affected that is shared by these duplications, [b] The size of she shared region denoted by range, [c] Small populations, [d] Large populations, [e] No antibiotics control populations, [f] Tetracycline only control populations. [g] Many duplications in this region appear to depend on recombination between rRNA sequences.

6. dN/dS and dI/dS analysis

To determine the role of natural selection, we considered the ratio of the rate of nonsynonymous to the rate of synonymous substitutions (dN/dS). To generate an expectation of the number of nonsynonymous and synonymous mutations that could occur within the whole genome (bacterial chromosome and pACTEM plasmid), we assumed a plasmid copy number of 10, and included the effect of mutational bias based on mutation accumulation data for *E. coli* [19]. We then determined the rate for each mutation class, by dividing the observed mutations by the expectation. We also considered the ratio of the rate of intergenic mutations to the rate of synonymous substitutions (dI/dS), as previously suggested [20], to get an indication of whether mutations in promotor regions were overrepresented in the data. To estimate the percentage of beneficial mutations, we assumed that all nonsynonymous or intergenic mutations that occur above the baseline substitution rate (as determined by the synonymous mutations) were beneficial, e.g. percentage beneficial mutations = 100*(dN/dS -1)/(dN/dS).

We generally found dN/dS and dI/dS values well above 1 for the non-mutator clones (**Supplementary Table 7**). By contrast, for the mutator clones dN/dS ~1, as expected for populations substituting mutations by chance. Large populations had appreciably higher dN/dS and dI/dS values than the other treatments, indicating stronger effects of selection in these populations.

Supplementary Table 7: Results of dN/dS and dI/dS analyses**.**

Clones	Populations	dN/dS	N beneficial	dI/dS	I beneficial
Mutators	All	1.302	23.2%	0.733	-
Non-mutators	All	13.789	92.7%	4.692	78.7%
	Small	11.938	91.6%	3.910	74.4%
	Large	28.830	96.5%	7.819	87.2%
	No antibiotic	6.234	84.2%	5.864	82.9%
	Tetracycline only	11.532	91.3%	5.864	82.9%

7. Repeatability of genomic changes

Methodology

We wanted to quantify how repeatable genome evolution was with metrics that could compare mutational events of all sizes, based on either (i) the exact position of mutations, or (ii) based on the genes modified by these mutations. We therefore formulated the *H*-index of repeatability, which for the pairwise comparison of a genotype *A* to *B* with *m* and *n* mutations, respectively, is:

$$H_{A,B} = \sum_{j=1}^{m}\sum_{k=1}^{n}\left(\frac{|A_j \cap B_k|}{|A_j|}\right) \Big/ \sum_{j=1}^{m}\sum_{l=1}^{m}\left(\frac{|A_j \cap A_l|}{|A_j|}\right) \quad (10)$$

The numerator measures the similarity between the mutational content of two genotypes by considering the positional overlap between mutations divided by the length of the reference (i.e., genotype A) mutation, and the denominator normalizes by the overlap between the mutational events within genotype A. E.g., a SNP can occur in a region that is duplicated in another genotype. As this metric is asymmetrical, the repeatability measure for the two genotypes is the mean of both reciprocal comparisons:

$$H = \frac{H_{A,B} + H_{B,A}}{2} \quad (11)$$

If the metric is performed with the exact coordinates of mutations, it is a nucleotide-level *H*-index, whereas if the genes affected by mutations are used, it is the gene-level *H*-index. When *H* is zero, there is no repeated evolution, whereas values of *H* of 1 represent convergence on the same genotype. For determining the *H*-index for *N* genotypes, we first determined the mean *H*-index for each genotype versus all other genotypes, and then performed further analyses on these data (as opposed to analyzing all pairwise *H*-indexes), avoiding inflation of the degrees of freedom. In **Supplementary Fig. 9** we provide several examples to illustrate how the index is calculated.

Nucleotide-level repeatability results

We determined nucleotide level *H*-indexes for clones from all evolved non-mutator populations, considering different classes of mutations. First, if all mutations are combined then *H*-indexes are lower for the small than for the large populations (**Supplementary Fig. 10A**). If we consider the *H*-index for the three different mutation classes (SNPs, Indels and SVs), it is apparent that different mutation classes drive overall repeatability of the small and large populations. In clones from the small populations, SVs show higher convergence than in clones from the large populations (**Supplementary Fig. 10B**). The control without antibiotics has a high overall *H*-index (**Supplementary Fig. 10A**), which is driven by SVs (**Supplementary Fig. 10B**), particularly the loss of the pACTEM plasmid in all lineages (**Supplementary Fig. 8**). The

tetracycline only control has a more similar profile to the large populations, with SNPs being more convergent than Indels or SVs (**Supplementary Fig. 10**). We also calculate *H*-indexes separately for the genome and plasmid (**Supplementary Table 8**). This analysis demonstrates that the convergent evolution seen for SNPs in the large populations occurs on both plasmid and bacterial chromosome, so it is not driven only by recurring mutations affecting the TEM-1 gene on the pACTEM plasmid.

Tenaillon et al. [20] report another statistic for quantifying the repeatability of molecular evolution, in which events that overlap for more than 10% of their length are considered to be repeated events, which we refer to as the *T*-index. The *H*-index and *T*-index are both asymmetrical and require reciprocal comparisons to be made between each pair of genotypes, but a possible advantage of the *H*-index is that it does not require the arbitrary choice of threshold value for overlap between events. We compared the two indexes for our data and found that they generally give very similar results (**Supplementary Fig. 11**).

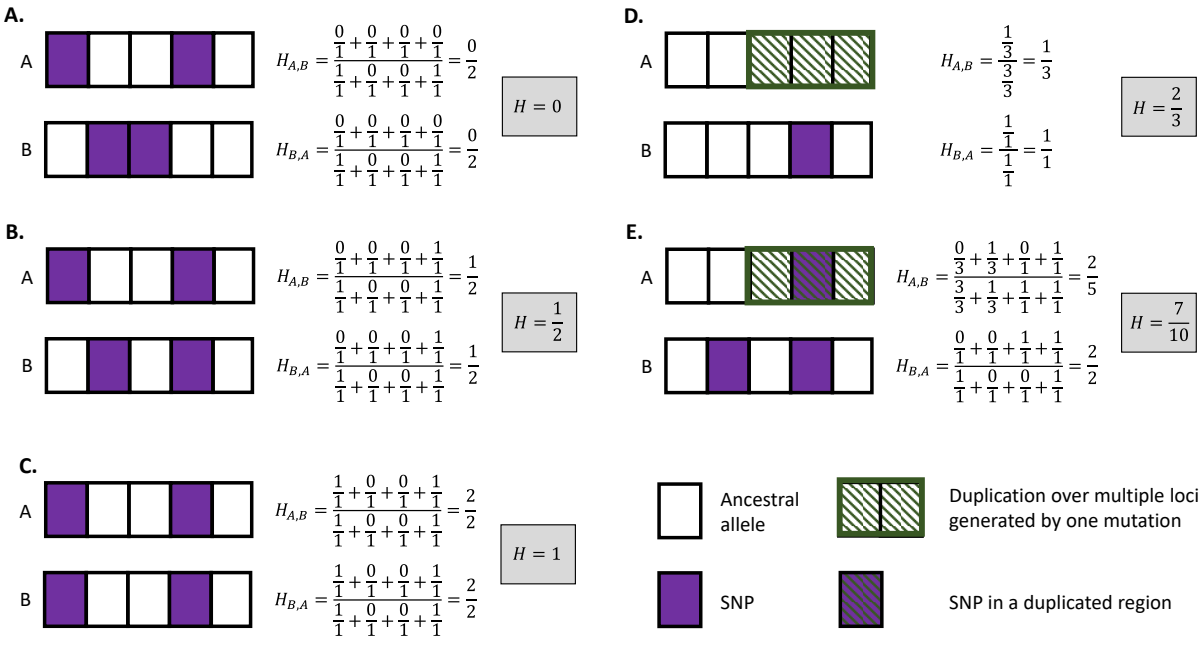

Supplementary Fig. 9: Examples of the calculation of *H*-index values. A genome with 5 loci is assumed, with genotypes "A" and "B" being used for each comparison. Purple coloring indicates a SNP (i.e., single nucleotide polymorphism), whereas the diagonal green patterns indicate a gene duplication. As a single gene duplication event extends over several loci, the green border surrounding the affected region indicates the duplication results from a single mutational event. The example genomes are presumed to be sequenced clones, in which all variation has been fixed. (A) Two genomes only carry SNPs at different loci, resulting in an $H = 0$. (B) Two genomes share a single SNP, while each carry a unique SNP, resulting in $H = ½$. (C) Two genomes are identical as they share two SNPs, resulting in $H = 1$. (D) Comparison of genomes

carry a SNP and gene duplication, which show some overlap. (E) A complex situation in which a SNP occurs within a duplicated region. Note that on rare occasions, $H > 1$ when such nested mutations occur and one of the mutations is shared between two genomes.

Gene-level repeatability results

We determined gene-level *H*-indexes for clones from all evolved non-mutator populations, considering different classes of mutations. As expected, gene-level repeatability was higher than nucleotide-level repeatability (**Extended Data Fig. 4**). One striking difference between the nucleotide-level and gene-level *H*-indexes is for the small populations, where repeatability for SNPs is much higher at the gene-level. Hence, although SNPs are less likely to affect the same nucleotide positions in small populations, they are likely to affect the same genes. As with the nucleotide-level *H*-indexes, the no antibiotics treatment has a higher repeatability than the tetracycline only treatment, although the no antibiotics treatment also has convergence for SNPs at the gene level (**Supplementary Fig. 10** and **Extended Data Fig. 4**). All calculated gene-level *H*-indexes are given in **Supplementary Table 9**.

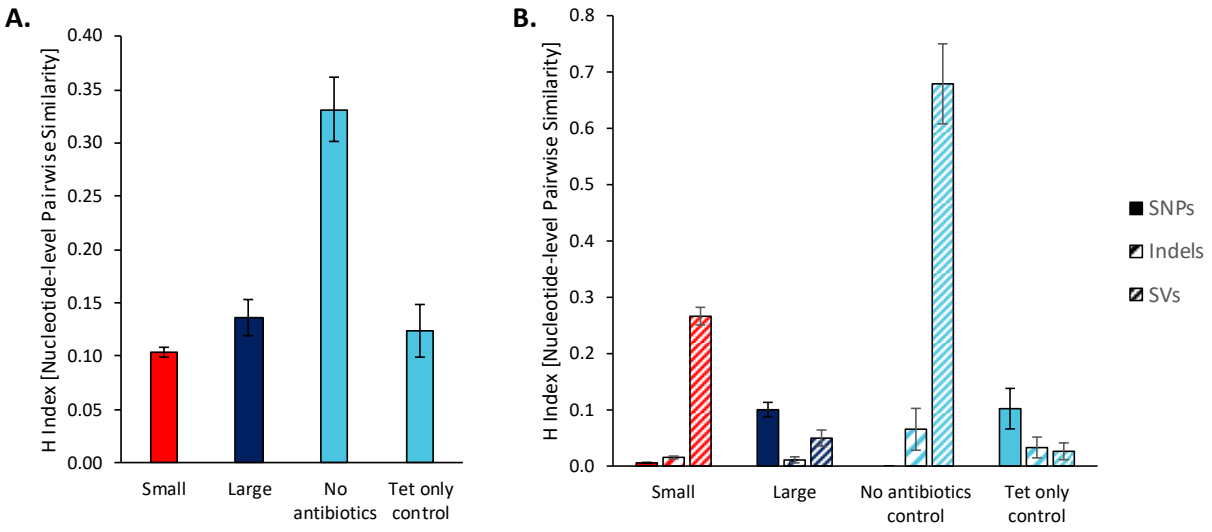

Supplementary Fig. 10: (**A**) Nucleotide-level *H*-index for all mutational events in clones from non-mutator populations. (**B**) Nucleotide-level *H*-index for three classes of mutational events, as indicated by the legend.

Supplementary Table 8: Nucleotide-level *H*-indexes for different loci (bacterial chromosome and the pACTEM plasmid) and different classes of mutations in clones from non-mutator populations. Mean *H*-index values ± standard error of the mean are given.

		Treatment			
Locus	Mutations	Small	Large	No antibiotics	Tetracycline
Both	All	0.104 ±0.005	0.136 ±0.075	0.331 ±0.030	0.124 ±0.025
Chromosome	All	0.068 ±0.003	0.070 ±0.011	0.176 ±0.032	0.116 ±0.024
Plasmid	All	0.361 ±0.029	0.352 ±0.043	1.000 ±0	0.132 ±0.048
Both	SNP	0.006 ±0.001	0.100 ±0.060	0 ±0	0.102 ±0.036
	Indel	0.015 ±0.002	0.011 ±0.005	0.066 ±0.037	0.033 ±0.019
	SV	0.266 ±0.133	0.050 ±0.014	0.679 ±0.071	0.026 ±0.015
Chromosome	SNP	0.006 ±0.001	0.070 ±0.016	0 ±0	0.118 ±0.040
	Indel	0.015 ±0.002	0.011 ±0.005	0.066 ±0.037	0.033 ±0.019
	SV	0.179 ±0.014	0.021 ±0.008	0.336 ±0.091	0.030 ±0.020
Plasmid	SNP	0.001 ±0.001	0.136 ±0.034	0 ±0	0 ±0
	Indel	0 ±0	0 ±0	0 ±0	0 ±0
	SV	0.285 ±0.032	0.048 ±0.019	1.000 ±0	0.010 ±0.007

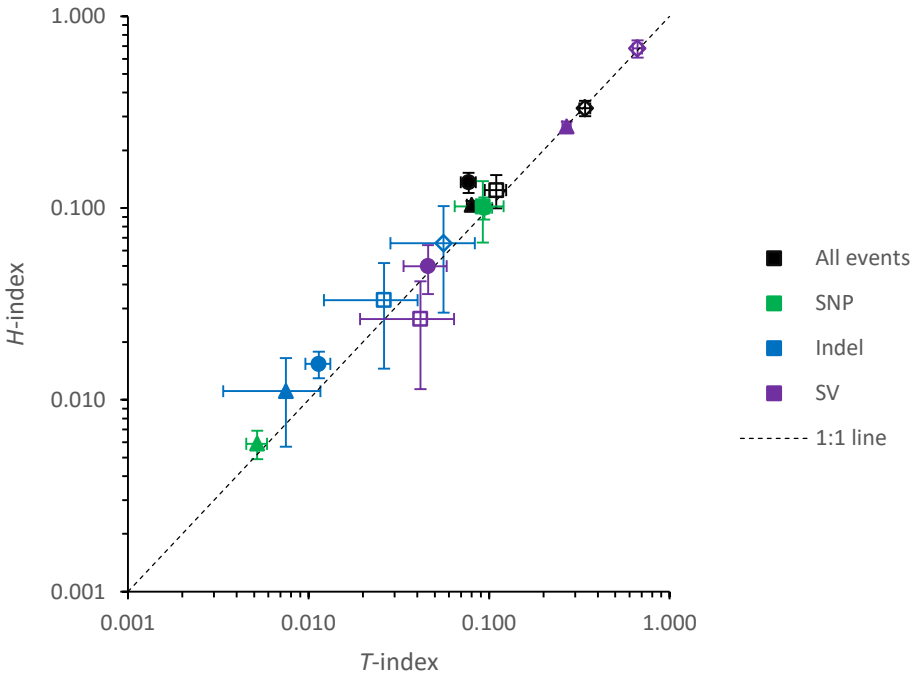

Supplementary Fig. 11: Comparison of the nucleotide-level *T* [20] and *H*-indexes for the final clone data. Each data point represents the mean *H*-index value for the small (filled triangles), large (filled circles), no antibiotics (open diamonds) or tetracycline only (open squares) treatments, for either all mutations (black), SNPs (green), Indels (blue) or SVs (purple), and error bars indicate the standard error of the mean. The 1:1 line is given as a reference only. For all the square-root-transformed mean *T* and *H*-indexes included in the figure, the coefficient of determination (r^2) is 0.983, indicating good agreement between the different indexes for these data.

Supplementary Table 9: Gene-level *H*-indexes for different loci (bacterial chromosome and the pACTEM plasmid) and different classes of mutations in clones from non-mutator populations. Mean *H*-index values ± standard error of the mean are given.

		Treatment			
Locus	Mutations	Small	Large	No antibiotics	Tetracycline
Both	All	0.310 ±0.010	0.458 ±0.018	0.488 ±0.042	0.281 ±0.070
Chromosome	All	0.284 ±0.010	0.407 ±0.039	0.358 ±0.052	0.249 ±0.064
Plasmid	All	0.448 ±0.038	0.831 ±0.125	1.000 ±0	0.321 ±0.100
Both	SNP	0.246 ±0.014	0.435 ±0.021	0.345 ±0.080	0.251 ±0.076
	Indel	0.046 ±0.007	0.084 ±0.021	0.107 ±0.033	0.009 ±0.006
	SV	0.267 ±0.018	0.049 ±0.015	0.668 ±0.050	0.032 ±0.021
Chromosome	SNP	0.251 ±0.015	0.386 ±0.050	0.345 ±0.080	0.231 ±0.068
	Indel	0.046 ±0.007	0.084 ±0.021	0.107 ±0.033	0.009 ±0.006
	SV	0.176 ±0.015	0.020 ±0.007	0.314 ±0.072	0.032 ±0.021
Plasmid	SNP	0.009 ±0.003	0.401 ±0.084	0 ±0	0.214 ±0.081
	Indel	0 ±0	0 ±0	0 ±0	0 ±0
	SV	0.287 ±0.032	0.048 ±0.019	1.000 ±0	0 ±0

8. Regression analysis of the relative frequency of SVs

To investigate whether the differences in selective conditions between small and large populations could explain the mutational repeatability pattern of SNPs and SVs, we performed linear regression analyses of the relationship between the fraction of SVs with respect to all mutations and the geometric mean of the CTX concentrations during the evolution experiment. Indeed, across all populations a significant dependence of the fraction of SVs on selective CTX concentrations is apparent (**Extended Data Fig. 5**, R^2=0.31, P<0.001). However, this dependence is not even approaching significance when considering either only small or large populations (Small; R^2=0.01, P=0.34, Large; R^2=0.02, P=0.59). Note that the lack of effect from selective CTX concentration among populations of the same size is not due to lack of variation in selective CTX concentration. This suggests that differences in mutation supply, and not differences in selective conditions, are responsible for the increased fraction of SVs in small populations. The regression analyses were performed using R version 3.6.1.

9. Dynamics of genomic changes

Muller plots

Population samples from different time points were analyzed with a metagenomics approach (see also "Detection of mutations for population samples" in section 2 of this document). A single clone from the final time point was also sequenced for each of these populations (see Section 4 "Overview of Genomics Data" of this document), and we checked whether the two sequencing results were congruent. If the final populations are polymorphic, we expect to detect some mutations only in the population and not all mutations detected in the population in the clone, which is congruent with our results for populations L1, L2, L5 and S4 (**Supplementary Table 10**). We expect that a small number of mutations may be detected in the clones but not in the populations because they were present at low frequency, and we indeed found a total of eight mutations only in the clones (**Supplementary Table 10**). By contrast, we expect to find mutations that are fixed in the population in the clones, which we found for 83 out of 85 cases (**Supplementary Table 10**). For the two mutations that were fixed in the meta-populations but not found in the clones, there was a reasonable explanation for why these discrepancies occurred (see footnotes in **Supplementary Table 10**). The data for the clones and populations are therefore generally in good agreement.

Using the combined clone and metapopulation sequencing results, we were able to determine the main haplotypes in the populations heuristically. For some of the small populations this was straightforward, as there was little clonal interference and most mutations detected fix successively along the single line of descent (S1, S14, S17 and S25). In other cases, the dynamics were more complex. The final clone data helped to identify the variants that coexisted for at least 200 generations in S4, and had similar frequencies at the time of measurement. In the large populations, at some time points there were multiple mutations that became extinct, and we could not establish whether there was linkage between them. For example, the multiple non-line-of-descent mutations in *acrB* appeared to occur on different read pairs, suggesting they were two different haplotypes, but this was an exceptional case. In other cases, mutations were assumed to be linked depending on the correlation of their frequencies. We used the *R* library *fishplot* [21] to visualize these data (**Fig. 4A**).

Repeatability of evolution

To determine whether the repeatability of the metagenomics results was similar to that obtained for the clones, we also estimated *H*-indexes for the time course data. We first performed this analysis for the majority mutations (frequency > 0.5) at the final time point (**Supplementary Fig. 12A**). This gave similar patterns for small and large populations to those observed for the clones (see Section 5 "Repeatability of

genomic changes"), albeit with more uncertainty due to the much smaller number of replicates. In the small populations, there was a high frequency of convergent SVs, whereas there were none in the large populations (**Supplementary Fig. 12A**). SNPs showed a higher repeatability in large than in small populations, although there was some convergence in the small populations driven by the occurrence of TEM mutations R241P in two of the small populations.

We also considered repeatability for all mutations detected – at any frequency – in the metagenomes over all time points, irrespective of their frequency, and hence fate (extinction or fixation). Here we saw patterns that were less divergent for the small and large populations, and strikingly SV repeatability was identical for both population sizes (**Supplementary Fig. 12B**). This finding suggests that the mutation supply of SV is similar in large and small populations, but that clonal interference with large-effect point mutations leads to the loss of beneficial SVs in large populations, in support of our hypothesis.

Supplementary Table 10: Comparison of mutations detected in clones and final populations. The number of mutations is given, with the percentage of all detected mutations per clone-population pair shown in parentheses.

	Unique mutations[a]			Shared mutations[b]	
	Clone	Population			
Population		Polymorphic	Fixed	Polymorphic	Fixed
L1	2 (14.3%)	5 (35.7%)	0 (0%)	0 (0%)	7 (50.0%)
L2	1 (6.7%)	4 (26.6%)	0 (0%)	3 (20.0%)	7 (46.7%)
L3	1 (8.3%)	0 (0%)	0 (0%)	0 (0%)	11 (91.7%)
L4	0 (0%)	0 (0%)	0 (0%)	0 (0%)	15 (100%)
L5	1 (12.5%)	1 (12.5%)	1 (12.5%)[c]	1 (12.5%)	4 (50.0%)
S1	0 (0%)	0 (0%)	1 (7.7%)[d]	1 (7.7%)	11 (84.6%)
S4	0 (0%)	3 (16.7%)	0 (0%)	10 (55.6%)	5 (27.8%)
S14	0 (0%)	0 (0%)	0 (0%)	0 (0%)	11 (100%)
S17	1 (11.1%)	0 (0%)	0 (0%)	0 (0%)	8 (88.9%)
S25	2 (22.2%)	0 (0%)	0 (0%)	0 (0%)	7 (77.8%)
Sum	8 (6.5)	14 (11.3)	2 (1.6)	17 (13.7)	83 (66.9)

[a] Mutations found only in the sequenced final clone or the meta-population. [b] Mutations found in both the

sequenced clone and meta-population. [c] The fixed mutation from the meta-populations that was not detected in the clone (10 base-pair deletion in *nlpI*), was present a frequency of 0.688 at 400 generations and 1.000 at 500 generations. Although our meta-population sequencing suggested that the mutation had gone to fixation (depth was only ≈ 24 at this site), in reality this mutation was at high frequency but not fixed and the clone represents a minority variant. [d] The duplication 4,013,902-4,146,518 was detected in the clone, but its frequency was too low to be considered reliable (1.3 fold increase in coverage). Given that this duplication was present in the meta-population, presumably a reversion of this duplication occurred during the culturing of the clone.

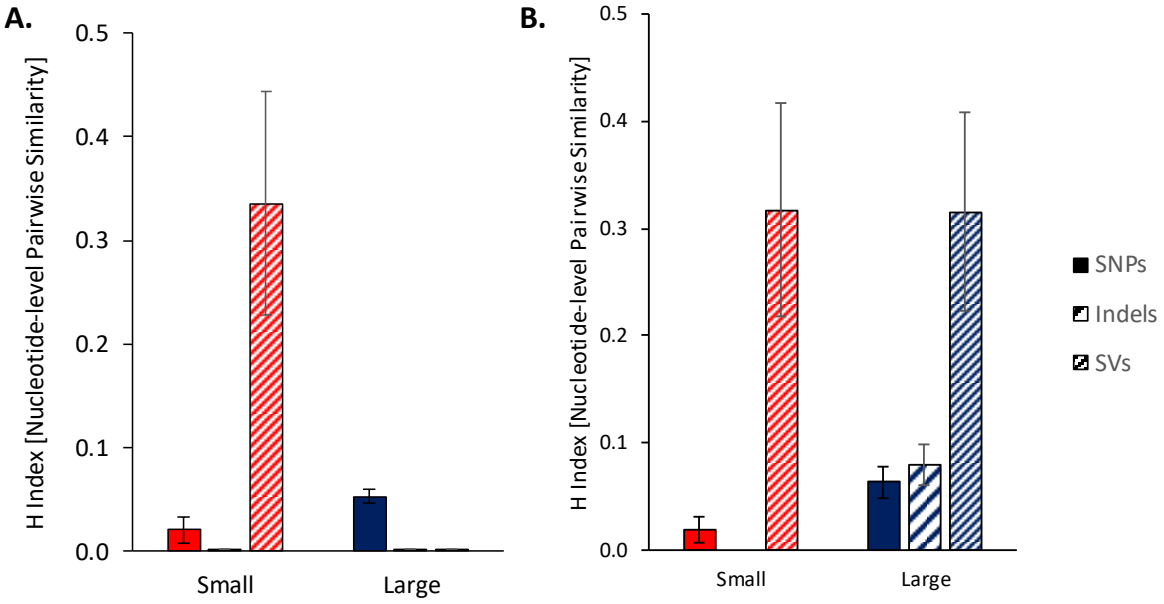

Supplementary Fig. 12. Nucleotide-level *H*-indexes for the five small and five large populations of **Fig. 4A** for which we obtained time-course meta-genome data, with fill pattern indicating the mutation category. (**A**) *H*-index for the majority mutations (frequency > 0.5) at the final time point. (**B**) *H*-index for all mutations detected at all timepoints, regardless of their frequency. Since the majority of detected mutations reach a majority frequency in the small populations, the indexes for detected and majority mutations are very similar. In the large populations, convergent SVs are detected, but clonal interference with large-effect SNPs prevents these mutations from fixing.

10. Inference of mutation parameters from Wright-Fisher simulations

We consider standard asexual Wright-Fisher (WF) dynamics [3] of a population where individuals can acquire beneficial mutations from three different classes. Mutations in each class occur randomly and independently with rates U_i per class $i = 1,2,3,$ individual and generation. The numbers of possible mutations for each class are given by $(L_1, L_2, L_3) = (20,6,6)$, which is sufficiently large such that the mutation supplies are not depleted at the end of the simulation for the parameter ranges expected to fit the experimental data. Thus the mutation rates for each single mutation are given by U_i/L_i. The genotypes τ of individuals in this model are encoded by three binary sequences τ_i of length L_i where each element is 1 or 0 indicating the presence or absence of the corresponding mutation. The selection coefficient of each mutation is chosen randomly from an exponential distribution [22] with mean s_i for mutation class i. A mutation with selection coefficient s increases the fitness f of the individual by a factor $1 + s$, and the effects of different mutations combine multiplicatively (no epistasis).

The WF dynamics is implemented as follows. At each time step t, the expected number of individuals of genotype τ at time $t + 1$ without selection is computed as:

$$P_{t+1}(\tau) = \left(1 - \sum_{i=1}^{3} U_i\right) N_t(\tau) + \sum_{i=1}^{3} \frac{U_i}{L_i} \sum_{j=1}^{L_i} N_t\left(\Delta_j^i \tau\right), \tag{12}$$

where $N_t(\tau)$ is the number of individuals of genotype τ in generation t and $\Delta_j^i \tau$ stands for the genotype obtained by flipping the j-th binary variable of τ_i. In the selection step, these numbers are then normalized with weights given by their fitness values $f(\tau)$,

$$\tilde{P}_{t+1}(\tau) = \frac{P_{t+1}(\tau) f(\tau)}{\sum_{\tau'} P_{t+1}(\tau') f(\tau')}. \tag{13}$$

The genotypes are finally sampled N times independently with a probability proportional to $\tilde{P}_{t+1}(\tau)$ to form a final population of total size N. The details of the algorithm are described in [23].

Following the setting of the experiment, we carried out WF simulations up to $t = 500$ generations for two different population sizes $N = 2 \times 10^6$ and $N = 2 \times 10^8$. Initially, the entire population is monomorphic for the wildtype genotype with fitness $f = 1$. Our aim is to determine the six model parameters $\{U_i, s_i\}_{i=1,2,3}$ such that the numbers of fixed mutations C_i for each class and each population size at the end point of the experiment are reproduced. This requires in principle to obtain the full distribution of $C = \left\{C_i^{small,large}\right\}_{i=1,2,3}$ and perform a likelihood

maximization. Unfortunately, since the statistics of C are accessible only through explicit simulations, this is a computationally daunting task that is not feasible in practice.

Instead, we approximate this distribution using a machine learning approach. Specifically, we use a so-called mixture density network with a Gaussian ansatz [24, 25]. We train the neural network to establish a functional relation:

$$g_w : \{U_i, s_i\}_{i=1,2,3} \to \left\{m_i^{small}, m_i^{large}, \sigma_i^{small}, \sigma_i^{large}\right\}_{i=1,2,3}, \tag{14}$$

where m_i and σ_i is the mean and the standard deviation of the random variable C_i. Correlations between the C_i values of different classes are neglected. The training procedure is implemented as follows. For an initially arbitrarily chosen parameter vector, which we call the center $\mathcal{P} = \{\ln U_i, s_i\}_{i=1,2,3}$, we create a cloud of parameter vectors $\mathcal{P}_i = \mathcal{P} + \xi_i$ of size 100, where the ξ_i values are randomly generated vectors. Then, for each parameter vector $\mathcal{P}_i$, we run two WF simulations to obtain C_i^{small} and C_i^{large} for the two different population sizes. This parameter-result pair is then added to the training set. Once this step is finished for the entire cloud, we train the neural network by maximizing

$$\mathcal{L} = \sum_i \left(\ln \text{Prob}^{\text{small}}\left(C_i^{\text{small}} \middle| \mathcal{P}_i\right) + \ln \text{Prob}^{\text{large}}\left(C_i^{\text{large}} \middle| \mathcal{P}_i\right)\right) \tag{15}$$

over the weights w, where $\text{Prob}(C_i|P_i)$ is a Gaussian distribution with parameters estimated from the network g_w.

After the training step, the next center is chosen to be the parameter vector with the largest log-likelihood for the empirical data. The whole process is repeated until the position of the center converges to a fixed value. By construction, this process only increases the size of training set (by 100 per iteration), and once the size of the training set is sufficiently large, it is expected that the neural network fully learns the distribution at least around the maximum.

In our actual implementation, we choose to approximate g_w as a fully connected feed-forward neural network with one hidden layer of 100 hidden units. The activation functions for these hidden neurons as well as the output neurons for the mean values m_i are chosen to be ReLU (rectified linear unit) activation functions. Since the standard deviations σ_i are positive by definition, this condition is imposed through exponential linear units. The random variables ξ_i for cloud generation are chosen to be Gaussian random vectors with standard deviation 0.1. The final size of the training set is reached at 10^5. We tested our approach by choosing different initial centers and found that they converged to the same final point. Finally, we performed a mini-batch optimization with Adam optimizer with an initial rate of 10^{-3}. The inferred model parameters are summarized in **Supplementary Table 11**, and **Extended Data Fig. 6** compares the distribution of

mutation numbers obtained from the WF model with optimized parameters to the experimental data.

Supplementary Table 11: Inferred mutation rates and selection coefficients for the three mutation classes.

	SNP	Indel	SV
U_i	2.17×10^{-8}	1.763×10^{-7}	7.051×10^{-6}
s_i	0.413	0.250	0.138

11. MIC effects of different mutation classes

For the clones from the evolved populations, we estimated MIC-effect sizes for different classes of mutations, using the genome data and CTX resistance data. To predict the effect size, we fit a series of general linear models to the data that predict the increase in resistance, Δ*R*, such that $\Delta R = log_2(MIC_{evolvedclone}) - log_2(MIC_{ancestor})$. There are 12 types of mutations possible (3 classes [SNP, Indel and SV] × 2 loci [chromosome and plasmid] × 2 population types [large and small]), so maximally 12 coefficients need to be estimated (**Supplementary Fig. 13**). In the simplest case, we assume all mutations have the same effect on MIC (Model 1), and therefore $\Delta R = \lambda q$ where λ is the effect-size coefficient (to be estimated from the data) and q is the total number of mutations of all types. Note there is no intercept in any of the models. Model 2 assumes mutations on the plasmid and chromosome – denoted by subscripts *p* and *c* – can have different effect sizes and hence $\Delta R = \lambda_c q_c + \lambda_p q_p$, and so forth for all models including the full model with 12 coefficients. All eight models were fitted to the data in R assuming a Normal distribution, and model selection was performed with the Akaike information criterion (AIC).

Model selection results are reported in **Supplementary Table 12**, and model parameter estimates are given in **Supplementary Table 13**. Model selection suggests that Models 4, 6 and 8 are the best-supported models. Model 8 appears to be over-parametrized, given it is the most complex and least well supported of the three models. Model 6 (which assumes differences between mutation effect size in large and small populations, on the bacterial chromosome and plasmid) essentially predicts that mutational effect size is larger for mutations in the plasmid than in the bacterial chromosome, and that mutations in plasmids from large populations have larger effect sizes than in plasmids from small populations. The model estimates therefore are being driven by TEM mutations and whilst highlighting their importance, they do not shed light on effect sizes for different classes of mutations. Model 4 (three mutation classes, separately for chromosome and plasmid) has a similar fit and level of support to Model 6, but includes mutation classes instead of population size, and is therefore the most informative model on the differences between effect size for different classes of mutations.

For model 4, SNPs have a highly significant effect on resistance (**Supplementary Table 13**), whereas the effect of SVs is marginally significant for the plasmid and insignificant for the bacterial chromosome. For events on the same locus, SNPs have a significant larger effect than SVs (*t* test; chromosome: $t = 2.094$, d.f. = 180, $P = 0.038$, plasmid: $t = 3.455$, d.f. = 180, $P < 0.001$). The effect of indels is intermediate, but estimates are poor for the plasmid due to the low number of indels that occur here. By contrast, the number of Indels on the chromosome is larger, but the effect size is not significantly different from either SNPs ($t = 0.692$, d.f. = 180, $P = 0.490$) or SVs ($t = 1.416$, d.f. = 180, $P = 0.158$).

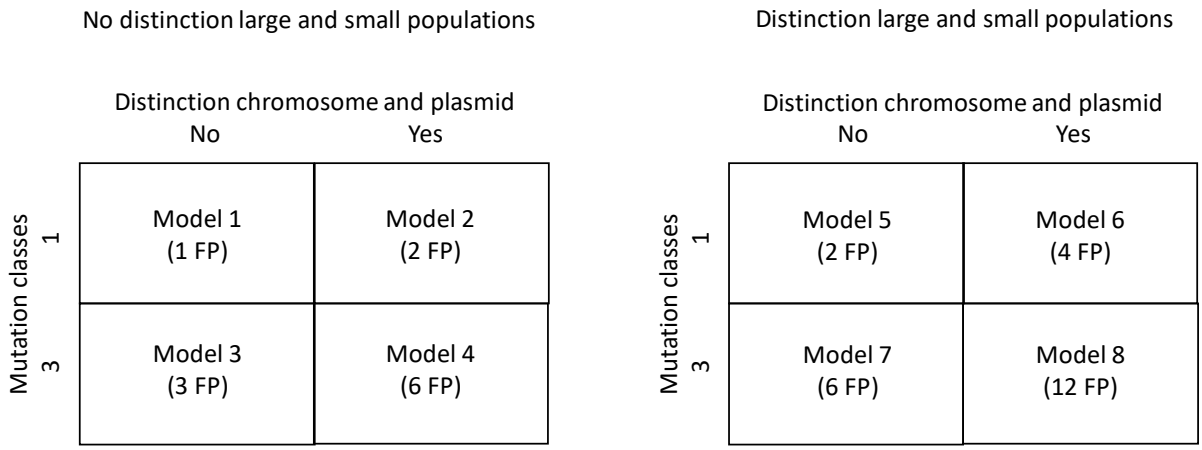

Supplementary Fig. 13: Overview of the eight different mutational effect-size models fitted to the MIC data. FP stand for “free parameters”. The three mutation classes used are SNP, Indel and SV.

Supplementary Table 12: Model selection with the AIC for effect sizes of mutation classes.

Model	Parameters	NLL	AIC	ΔAIC
1	1	240.239	484.48	70.90
2	2	212.816	431.63	18.05
3	3	228.313	464.63	51.05
4	6	201.668	417.34	3.76
5	2	212.239	432.48	18.90
6	4	200.790	413.58	-
7	6	209.045	434.09	20.51
8	12	195.460	418.92	5.34

Supplementary Table 13: Estimated model parameters and their standard errors of the mean (SEM). Subscripts c and p denote the chromosome or plasmid, and subscripts *snp*, *ind* and *sv* refer to SNP, Indels and IS-element insertions and SVs, respectively. For models 5-8 the parameter estimates are made separately for large and small populations. Significance levels for one-sample *t* tests against a value of zero are indicated by asterisks: *** $P < 0.001$, ** $P < 0.01$, * $P < 0.05$.

Model	Parameter estimate ±SEM
1	$\lambda = 0.835 \pm 0.035$***
2	$\lambda_c = 0.589 \pm 0.039$***, $\lambda_p = 3.087 \pm 0.263$***
3	$\lambda_{snp} = 1.230 \pm 0.096$***, $\lambda_{ind} = 0.717 \pm 0.189$***, $\lambda_{sv} = -0.132 \pm 0.204$
4	$\lambda_{c,snp} = 0.803 \pm 0.094$***, $\lambda_{c,ind} = 0.684 \pm 0.144$***, $\lambda_{c,sv} = 0.327 \pm 0.207$, $\lambda_{p,snp} = 3.180 \pm 0.250$***, $\lambda_{p,ind} = 0.530 \pm 1.707$, $\lambda_{p,sv} = 1.193 \pm 0.518$*
5	Large: $\lambda = 1.136 \pm 0.099$***; Small $\lambda = 0.729 \pm 0.025$***
6	Large: $\lambda_c = 0.709 \pm 0.110$***, $\lambda_p = 3.255 \pm 0.435$***; Small: $\lambda_c = 0.651 \pm 0.041$***, $\lambda_p = 1.702 \pm 0.408$***
7	Large: $\lambda_{snp} = 1.310 \pm 0.252$***, $\lambda_{ind} = 1.140 \pm 0.788$, $\lambda_{sv} = -0.235 \pm 1.156$; Small: $\lambda_{snp} = 0.890 \pm 0.102$***, $\lambda_{ind} = 0.759 \pm 0.140$***, $\lambda_{sv} = 0.355 \pm 0.175$*
8	Large: $\lambda_{c,snp} = 0.691 \pm 0.274$*, $\lambda_{c,ind} = 1.126 \pm 0.638$, $\lambda_{c,sv} = 0.283 \pm 1.321$, $\lambda_{p,snp} = 3.208 \pm 0.481$***, $\lambda_{p,ind} = -0.684 \pm 4.103$, $\lambda_{p,sv} = 2.652 \pm 2.850$; Small: $\lambda_{c,snp} = 0.775 \pm 0.107$***, $\lambda_{c,ind} = 0.690 \pm 0.138$***, $\lambda_{c,sv} = 0.387 \pm 0.205$, $\lambda_{p,snp} = 2.392 \pm 0.560$***, $\lambda_{p,ind} = 1.048 \pm 2.006$, $\lambda_{p,sv} = 1.110 \pm 0.480$*

12. Analysis of functional targets and evolutionary trajectories

We defined functional targets, and their likely adaptive role in our evolution experiment, by grouping genes affected by at least five SNPs and/or indels in the 96 CTX-treated populations, based on information about their function and regulation in EcoCyc (ecocyc.org) and literature (references inserted below), as well as the types of mutations involved (see **Supplementary Table 14**).

1. AcrAB-TolC upregulation. AcrAB-TolC is the paradigm efflux pump of the RND family of multidrug efflux pumps [26]. AcrB is the innermembrane structural component of the pump, while AcrR is a negative regulator of the AcrAB operon and PhoQ is a positive regulator of TolC, the outermembrane component of the pump [26]. We found a total of 111 SNPs and indels in *acrB*, *acrR* and *phoQ* in the 96 CTX-treated populations, and only one in the eight tetracycline-treated populations, suggesting that the pump has little affinity for tetracycline. Further, AcrB has a transmembrane and periplasmic domain and determines the pump's specificity [26]. Because only one of the 61 mutations affecting this gene inactivates the gene (one small population has a frameshift mutation), it is likely that these mutations either enhance the affinity for CTX. Mutations in *acrR* include several frameshift and nonsense mutations, consistent with its role in repressing expression of *acrAB*, while all eight mutations in *phoQ* are nonsynonymous SNPs, which presumably enhance expression of TolC [26]. Therefore, mutations in *acrR*, *acrB* and *phoQ* all seem to be involved in the upregulation of AcrAB-TolC and increasing its affinity for CTX.
2. Downregulation of plasmid copy number. The copy number of plasmid pACTEM is low (~10 copies/cell) due to relaxed regulation of its p15A origin of replication (ori) [27]. Inactivating mutations in *pcnB* and *polA* have been found to decrease copy number of plasmids with related p15A ori [28]. Because the mutations in *pcnB* and *polA* likely inactivated both gene functions (they include frameshift mutations and stop codons), and since lowered copy number was expected to be beneficial given that TEM1 β-lactamase was expressed from a strong pTac promoter and derepressed with IPTG, we expected these mutations to have decreased plasmid copy number. To test this, we compared TEM expression levels of the evolved clones from the 24 large populations, in which the plasmid was replaced by the ancestral pACTEM1 plasmid, with those in the two ancestral strains, using nitrocefin assays (see SM section 3, Experimental methods and results: "TEM β-lactamase activity assays"). The clone from population L18 was the only one without mutations in either *pcnB* or *polA*, and the clones from this population and population L5 (which had a 210-bp deletion in *pcnB*) were the only two showing lower β-lactamase expression than the ancestral strains (see **Supplementary Fig. 3**). Therefore, the mutations inactivating *pcnB* and *polA* likely provided a fitness benefit by down-regulating plasmid copy number.
3. Transcription regulation. MarR is a DNA-binding transcriptional repressor involved in the regulation of many biological processes, including antibiotic resistance [29]. The 42 SNPs and indels affecting *marR*

include many nonsense and frame-shift mutations. Inactivation of MarR is expected to both upregulate AcrAB-TolC efflux and downregulate OmpF [26]. SlyA is a related transcription factor involved in the regulation of virulence, the silencing of horizontally acquired genes and repression of small-molecule efflux systems [30]. The mutations we observed inactivate SlyA and occur only in CTX-treated populations, suggesting that they may enhance CTX efflux. Non-synonymous SNPs in *rpoB* and *rpoD*, at different positions from those we found in our clones, have recently been reported to increase resistance to the cephalosporin ceftriaxole in *Neisseria ghonorrhoeae* [31]. DNA gyrase is not known for its role in β-lactam resistance. Mutations in *rpoABCD* and *gyrAB* were found only in the CTX-treated populations and did not include nonsense or frame-shift mutations. Moreover, two clones had the same Val771Gly mutation in *gyrA* and six clones had mutations at the same position in *rpoD* (of which four shared Asp445Glu), indicating selective benefits associated with changes in the regulation of gene expression.

4. OmpF downregulation. OmpF is the major outermembrane porin in *E. coli* B, and involved in the influx of β-lactams and other antibiotics [32]. The fact that *ompF* is deleted also in seven of the eight control populations challenged with tetracycline only, suggests tetracycline also enters through this porin. EnvZ-OmpR is a two-component regulatory system involved in the response to changes in osmolarity and positively regulating the expression of OmpF [32]. Since the mutations affecting all three genes include inactivating mutations, such as frameshift and nonsense mutations, mutations affecting *ompF*, *ompR* and *envZ* likely downregulate or abolish expression of OmpF.
5. Target alteration. Penicillin-binding protein 3 (PBP3), encoded by *ftsI*, is a transpeptidase catalyzing the final step of cell-wall biosynthesis by cross-linking peptidoglycan strands. It is also the main target to which CTX binds [33], which results in the inhibition of cell-wall synthesis and further toxic downstream effects [34]. Of the 58 mutations affecting *ftsI*, 56 were nonsynonymous SNPs and two in-frame (3-bp) indels. Moreover, we found high repeatability of mutations at the nucleotide level, with mutations at nine amino-acid positions occurring in more than one population, including 12 at position 536 (all Glu536Leu) and nine at position 167 (all Arg167Cys). At positions 311 (4 clones) and 545 (1 clone) mutations were also found in a previous study using CTX selection [33]. These PBP3 mutations, therefore, provide clear selective benefits, most likely by reducing CTX binding, while in theory -- since PBP's are evolutionary related to β-lactamases – some of these mutations might enhance the hydrolysis of CTX [33].
6. TEM deletion. All but two of the 45 deletions affecting TEM1 β-lactamase involved the 2,374-bp full deletion of bla_{TEM1} and its repressor *lacI* from the plasmid (**Figs. 2C**); in two small populations, smaller deletions partially removing bla_{TEM1} and its promoter were observed. All deletions are thus expected to fully cancel expression of TEM1. The bla_{TEM1} and *lacI* loci are deleted by a single recombination event mediated by two homologous 185-bp sequences up and downstream of the two adjacent genes in the pACTEM1 plasmid. The deletion of these two genes is not driven by a selective benefit (**Fig. 4D**), but by a high deletion rate and genetic hitchhiking with beneficial mutations. Consistent with this scenario, in

the five populations with time-resolved information where the TEM deletion occurs (populations S1, S14, L2, L3 and L5, **Fig. 4A**), it always spreads together with other mutations. Moreover, this deletion occurred at similar frequency in the large CTX-treated populations (6/24) and eight control populations that were treated with tetracycline only (2/8, see **Supplementary Fig. 8**; the eight large control populations without antibiotics all lost the entire plasmid). Since the selective conditions likely differ between CTX-treated and control populations, a neutral effect of the TEM deletion would be the simplest explanation for these observations.

7. TEM activation. Besides the common deletion of *bla*$_{TEM1}$ and *lacI* and six *bla*$_{TEM1}$ promoter mutations (see above), 32 of the remaining 33 other mutations affecting TEM1 β-lactamase were nonsynonymous SNPs (the remaining mutation was a frameshift indel in a small population). The 32 SNPs are all known from clinical and/or laboratory studies [35], and show remarkable convergence, with 28 shared by multiple clones. These include known largest-benefit mutation Gly238Ser [16], shared by clones from 13 populations, and mutations at amino-acid positions 104, 164, 240, 241 and 265, shared by at least two clones. Eight large and two small populations had at least two SNPs in *bla*$_{TEM}$, including known adaptive combinations of Gly238Ser with Glu104Lys (3x) and Thr265Met (2x), and Arg164Ser with Ala237Thr [36]. Clearly, these mutations provided substantial fitness benefits by enhancing TEM's activity against CTX (see e.g. **Fig. 4D**).
8. Upregulation of outer-membrane vesicles. NlpI is an outer-membrane-anchored lipoprotein, whose inactivation is known to enhance β-lactam resistance and increase the production of outer-membrane vesicles (OMVs) [37], as well as upregulate PBP4 during log phase and Spr during stationary phase [38]. Increased production of OMVs is thought to protect against stressors targeting the outer membrane via absorption [39]. Recently, the protective effect of OMVs against β-lactams such as CTX was shown to depend on the expression of an active β-lactamase [40]. Consistent with this scenario, the mutations we observed inactivated NlpI and were positively associated with TEM-activating SNPs (**Fig. 5B**). Therefore, we expect that the benefit of *nlpI*-inactivating mutations in our populations resulted from the more effective removal of CTX via the increased production of OMVs.
9. TEM expression. The six mutations occurring upstream of *bla*$_{TEM1}$ occur all in the Tac promoter region (80-11bp upstream of the transcription start site), ranging from position -59 to -19, and including two at the same position (-41). It is unclear whether they increased or decreased expression of TEM β-lactamase. The strain we used has a copy of *lacI*, the gene encoding the LacI repressor of *bla*$_{TEM}$, both in the chromosome and on plasmid pACTEM. In total 16 SNPs and 25 large chromosomal deletions affect at least one *lacI* copy across the 96 populations (in addition to 45 combined deletions of *bla*$_{TEM1}$ and *lacI* from the plasmid). The deletion varied in size from 17,365-55,080 bp and affected at least 14 other genes (**Supplementary Table 5**) and also occurred in one of the control populations that lost the pACTEM plasmid. Moreover, no frameshift or nonsense mutations affecting *lacI* were observed (which would upregulate TEM expression), and at three amino-acid positions mutations were observed in two

populations. Furthermore, we know that a majority of populations have mutations in *pcnB* or *polA* that lower TEM expression (**Supplementary Fig. 3**), presumably by lowering plasmid copy number, suggesting lower TEM expression is adaptive. Therefore, we expect that the *lacI* mutations downregulate TEM expression, either through weaker binding of LacI to lactose analog IPTG or tighter binding to the bla_{TEM1} promoter. This would imply that the large deletions removing *lacI* may not provide a fitness benefit, at least not due to the removal of *lacI*.

We then looked for associations among mutations affecting these nine functional targets, in order to reveal possible adaptive trajectories in our populations, following the approach of Tenaillon et al. [20]. We excluded SVs from this analysis, because their adaptive role is unclear. However, we did include the deletion of *TEM*, as this particular SV is a highly repeated event with clear adaptive consequences (**Fig. 5**). We looked for interactions between functional targets using two approaches: (1) a Spearman rank correlation (ρ) between all functional units, and (2) Lewontin's normalized coefficient of linkage disequilibrium (*D'*) [37]. Whereas different mutational trajectories are evident for the large populations, for the small populations this is not the case (**Fig. 5**).

Analysis of evolutionary trajectories

To identify evolutionary trajectories we looked for associations between the mutations assigned to these nine functional targets, following the approach of Tenaillon et al. [20]. We were particularly interested in the effects of the TEM deletion and TEM activation on the trajectory followed. There were no clear associations for small populations, whereas large populations revealed two alternative trajectories (**Fig. 5B**) which had adaptive consequences, affecting the resistance levels (**Fig. 5C+D**).

Supplementary Table 14. Functional targets based on mutations affecting multiple-hit genes in the 96 CTX-treated populations.

	Functional target	Gene	GoF/ LoF[1]	SNP[2]			Indel/IS insertion		SV		**Total number**
				Syn	NonSyn[3]	Reg	Coding	Reg	Deletion (>1kbp)	Duplication (>1kbp)	
1.	AcrAB-TolC upregulation	*acrB*	G	0/0	43/16	0/0	1/1	0/0	0/0	6/0	**50/17**
		acrR	L	0/0	17(3*)/7(1*)	2/0	13/3	0/0	1/0	4/0	**37/10**
		phoQ		0/0	4/4	0/0	0/0	0/0	0/0	0/0	**4/4**
2.	Downregulation plasmid copy number	*pcnB*	L	1/0	52(9*)/14(1*)	0/2	14/6	2/0	0/0	0/0	**69/22**
		polA		0/0	5/2	0/0	1/0	0/0	0/0	15/2	**21/4**
3.	Transcription regulation	*marR*	L	1/0	15(2*)/4	2/0	3/0	15/2	0/0	1/0	**37/6**
		slyA		0/0	8(1*)/1(1*)	0/0	5/0	2/0	0/0	0/0	**15/1**
		gyrAB		0/1	12/1	0/0	1[6]//0	0/0	0/0	2/0	**15/2**
		rpoABCD	G[8]	0/0	15/7	0/0	0/0	0/0	0/0	0/0	**15/7**
4.	OmpF downregulation	*ompR*	L	0/0	19(3*)/4	0/0	9/1	1/2	1/0	1/0	**31/7**
		ompF		0/0	8(2*)/0	3/0	4/1	4/2	0/0	0/0	**19/3**
		envZ	L	0/0	9(1*)/8(4*)	0/0	2/4	0/0	2/0	0/0	**13/12**
5.	Target alteration	*ftsI*	G	0/0	23/33	0/0	2[7]/0	0/0	0/0	0/0	**25/33**
6.	TEM deletion[3]	*lacI*							39/6		**39/6**
		bla_{TEM}									
7.	TEM activation[3]	bla_{TEM}	G		7/25						**7/25**
8.	Upreg of outer-membrane vesicles	*nlpI*		0/0	3(2*)/4(1*)	0/0	9/9	0/1	0/0	0/0	**12/14**
9.	TEM expression[4]	*lacI*	G	0/0	8/8	0/0	0/0	0/0	21/4[5]	0/0	**29/12**
		bla_{TEM}		0/0		0/6	0/0	1/0		0/0	**1/6**
	Total			**2/1**	**248(23*)/138(8*)**	**7/8**	**64/25**	**25/7**	**64/10**	**29/2**	**439/191**

[1] Classification of genes as having gain-of-function (GoF, indicated with a G) or loss-of-function (LoF, indicated with an L) mutations, based on mutational patterns and gene functions (for details see Section 13: Analysis of gain- and loss-of-function mutational patterns). Only genes in which >10 SNPs are included in the classification. [2] Mutation numbers for Small/Large populations, respectively. Syn: synonymous, NonSyn: nonsynonymous, Reg: mutation in putative regulatory sequence of gene. [3] (*) indicate nonsense mutations. [4] For the *lacI* and bla_{TEM} genes, each mutation class is assigned to a different functional target. Grey shading indicates mutation classes that are not compatible with the functional target. [5] Deletions of chromosomal *lacI* copy. [6] An in-frame 6-bp insertion. [7] Both indels are 3-bp in-frame deletions. [8] Of the genes in this operon, only *rpoD* had >10 SNPs and therefore only *rpoD* is classified as GoF.

13. Analysis of gain-of-function and loss-of-function SNPs

Individual genes from the functional targets (**Supplementary Table 14**), identified by considering multiple mutational hits, were classified as having mutations that introduced a gain or alteration of function (Gof) or loss of function (LoF). To be included in this classification and subsequent analyses, genes had to have >10 SNPs in their coding region in all small and large populations, including at least 2 SNPs for each population size. For the 10 genes which met these criteria, we considered the following criteria to classify them as targets for GoF or LoF.

1. To be classified as GoF targets, genes can have a maximum of 1 mutation that is unambiguously associated with a LoF per population size. Mutations associated with LoF are:
    (a) SNPs resulting in frameshifts
    (b) Indels or IS inserts, with the exception of short (≤ 30 bp) insertions or deletions that conserve the reading frame.
    (c) SVs that partially or wholly remove the gene (i.e., genomic deletions)
2. The GoF/LoF classification should be consistent with what is known about the function of the gene.

For all genes with sufficient SNPs to be considered here, there is some information on their function (see Section 12: Analysis of functional targets and evolutionary trajectories). When considering the second criterion for the 5 genes that meet criterion 1 for GoF (bla_{TEM1}, *ftsI, acrB, lacI* and *rpoD*), GoF mutations are known to occur and can be linked to benefits in two genes; bla_{TEM1}: enhanced catalytic function, and *ftsI*: reduced CTX binding by alteration of the target site. For two genes, there is a plausible mechanism suggesting GoF mutations could be important; *acrB*: this is an essential component of the AcrAB-TolC efflux pump, whose modification likely enhances the affinity for CTX (or tetracycline); and *lacI*: reduction of TEM expression by enhanced binding and repression of the Tac promoter, because increased TEM expression requires inactivation of LacI (which we did not observe) and reduced TEM expression is likely beneficial for growth given the high expression from the Ptac promoter and derepression with IPTG in our experiment. For *rpoD*, there is considerable convergent evolution (6 clones had mutations at the same position), but a plausible mechanism is unclear as this sigma initiation factor affects many genes related to fast growth.

For the genes identified as LoF by criterion 1 (*acrR, pcnB, marR, ompR* and *envZ*), there are two transcriptional regulators where LoF mutations are known to have benefits in the presence of antibiotics (*acrR, marR*), two genes are part of a two-component sensor that regulates expression of a porin involved in the influx of antibiotics (*ompR* and *envZ*), and inactivation of *pcnB* decreases plasmid copy number of the p15A ori, presumably leading to lower TEM expression (**Supplementary Fig. 3**). Therefore, the classification of these 10 genes as GoF or LoF targets is consistent with what is known

about these genes, although in the case of *rpoD* a putative mechanisms remains unclear.

To consider the repeatability of mutations in the 10 genes included in the GoF/LoF analysis, for individual genes we calculated the nucleotide level H-index for SNPs only (see Section 7: Repeatability of genomic changes). The calculation of these H-indexes was performed only for those final clones that carried SNPs in a particular gene.

Finally, to get an indication of the magnitude of mutational effects for GoF and LoF SNPs, we fitted a general linear model to the data following the approach described previously (see Section 11, MIC effects of different mutation classes). Indels and SVs were included as separate classes of mutations in the model, and SNPs were subdivided into SNPs outside the functional targets (**Supplementary Table 14**), LoF and GoF. In addition, a model was used where TEM and GoF without TEM were used as separate categories, in addition to the other mutation class categories. Their mutational effects on MIC were estimated using general linear models as implemented in R 3.6.1 ('glm'-function; base package). Model fit was assessed by visual inspection of the homogeneity of residuals ('simulateResiduals'-function; DHARMa package). Estimates were obtained for two models: one including GoF (w/o TEM), LoF, TEM, Plasmid and chromosomal indels, Plasmid SVs and chromosomal SVs, the other included GoF, LoF, Plasmid and chromosomal indels, Plasmid SVs and chromosomal SVs as explanatory variables. Significant differences between coefficient estimates were evaluated using a Wald Chi-Squared test ('linearhypothesis'-function; car package).

References

1. Gerrish, P.J. and R.E. Lenski, *The fate of competing beneficial mutations in an asexual population.* Genetica, 1998. **102/103**: p. 127-144.
2. Good, B.H., et al., *Distribution of fixed beneficial mutations and the rate of adaptation in asexual populations.* Proceedings of the National Academy of Sciences USA, 2012. **109**: p. 4950–4955.
3. Park, S.-C., D. Simon, and J. Krug, *The speed of evolution in large asexual populations.* Journal of Statistical Physics, 2010. **138**: p. 381-410.
4. Good, B.H. and M.M. Desai, *Deleterious Passengers in Adapting Populations.* Genetics, 2014. **198**(3): p. 1183-1208.
5. Schiffels, S., et al., *Emergent Neutrality in Adaptive Asexual Evolution.* Genetics, 2011. **189**: p. 1361–1375.
6. McCandlish, D.M. and A. Stoltzfus, *Modeling Evolution Using the Probability of Fixation: History and Implications.* The Quarterly Review of Biology, 2014. **89**(3): p. 225-252.
7. Yampolsky, L.Y. and A. Stoltzfus, *Bias in the introduction of variation as an orienting factor in evolution.* Evolution & Development, 2001. **3**(2): p. 73-83.
8. Jain, K., J. Krug, and S.-C. Park, *Evolutionary advantage of small populations on complex fitness landscapes.* Evolution, 2011. **65**: p. 1945–1955.
9. Svensson, E.I. and D. Berger, *The Role of Mutation Bias in Adaptive Evolution.* Trends in Ecology & Evolution, 2019. **34**(5): p. 422-434.
10. Gomez, K., J. Bertram, and J. Masel, *Mutation bias can shape adaptation in large asexual populations experiencing clonal interference.* Proceedings of the Royal Society B: Biological Sciences, 2020. **287**(1937): p. 20201503.
11. Lenski, R.E., et al., *Long-term experimental evolution in Escherichia coli. I. Adaptation and divergence during 2,000 generations.* American Naturalist, 1991. **138**: p. 1315-1341.
12. Martin, M., *Cutadapt removes adapter sequences from high-throughput sequencing reads.* EMBnet.journal, 2011. **17**(1): p. 10-11.
13. Bolger, A.M., M. Lohse, and B. Usadel, *Trimmomatic: A flexible trimmer for Illumina Sequence Data.* Bioinformatics, 2014. **30**(15): p. 2114-2120.
14. Langmead, B. and S.L. Salzberg, *Fast gapped-read alignment with Bowtie 2.* Nature Methods, 2012. **9**(4): p. 357-359.
15. Li, H., et al., *The Sequence Alignment/Map format and SAMtools.* Bioinformatics, 2009. **25**(16): p. 2078-2079.
16. Schenk, M.F., et al., *Quantifying the adaptive potential of an antibiotic resistance enzyme.* PLoS Genetics, 2012. **8**: p. e1002783.
17. Park, S.-C. and J. Krug, *Clonal interference in large populations.* Proceedings of the National Academy of Sciences USA, 2007. **104**: p. 18135-18140.
18. de Visser, J.A.G.M., et al., *Diminishing returns from mutation supply rate in asexual populations.* Science, 1999. **283**: p. 404-406.
19. Lee, H., et al., *Rate and molecular spectrum of spontaneous mutations in the bacterium Escherichia coli as determined by whole-genome sequencing.* Proceedings of the National Academy of Sciences, 2012. **109**: p. E2774–E2783.
20. Tenaillon, O., et al., *The Molecular Diversity of Adaptive Convergence.* Science, 2012. **335**: p. 457-461.
21. Miller, C.A., et al., *Visualizing tumor evolution with the fishplot package for R.* BMC Genomics, 2016. **17**(1): p. 880.
22. Orr, H.A., *The distribution of fitness effects among beneficial mutations.* Genetics, 2003. **163**: p. 1519-1526.
23. Nowak, S., et al., *Multidimensional Epistasis and the Transitory Advantage of Sex.* PLoS Comput Biol, 2014. **10**(9): p. e1003836.

24. Bishop, C.M., *Mixture density networks*. 1994, Birmingham: Aston University.
25. Bishop, C.M., *Pattern Recognition and Machine Learning*. 2011, New York: Springer.
26. Du, D., et al., *Multidrug efflux pumps: structure, function and regulation.* Nature Reviews Microbiology, 2018. **16**(9): p. 523-539.
27. Barlow, M. and B.G. Hall, *Predicting evolutionary potential: In vitro evolution accurately reproduces natural evolution of the TEM beta-lactamase.* Genetics, 2002. **160**: p. 823-832.
28. Chakravartty, V. and J.E. Cronan, *A series of medium and high copy number arabinose-inducible Escherichia coli expression vectors compatible with pBR322 and pACYC184.* Plasmid, 2015. **81**: p. 21-26.
29. Ellison, D.W. and V.L. Miller, *Regulation of virulence by members of the MarR/SlyA family.* Current Opinion in Microbiology, 2006. **9**(2): p. 153-159.
30. Will, W.R., et al., *The Evolution of SlyA/RovA Transcription Factors from Repressors to Countersilencers in Enterobacteriaceae.* mBio, 2019. **10**(2): p. e00009-19.
31. Palace, S.G., et al., *RNA polymerase mutations cause cephalosporin resistance in clinical Neisseria gonorrhoeae isolates.* eLife, 2020. **9**: p. e51407.
32. Choi, U. and C.-R. Lee, *Distinct Roles of Outer Membrane Porins in Antibiotic Resistance and Membrane Integrity in Escherichia coli.* Frontiers in microbiology, 2019. **10**: p. 953-953.
33. Sun, S., M. Selmer, and D.I. Andersson, *Resistance to b-Lactam Antibiotics Conferred by Point Mutations in Penicillin-Binding Proteins PBP3, PBP4 and PBP6 in Salmonella enterica.* PLoS One, 2014. **9**: p. e97202.
34. Cho, H., T. Uehara, and Thomas G. Bernhardt, *Beta-Lactam Antibiotics Induce a Lethal Malfunctioning of the Bacterial Cell Wall Synthesis Machinery.* Cell, 2014. **159**(6): p. 1300-1311.
35. Salverda, M.L.M., J.A.G.M. de Visser, and M. Barlow, *Natural evolution of TEM-1 beta-lactamase: experimental reconstruction and clinical relevance* FEMS Microbiology Reviews, 2010. **34**: p. 1015–1036.
36. Salverda, M.L.M., et al., *Initial mutations direct alternative pathways of protein evolution.* PLoS Genetics, 2011. **7**(3): p. e1001321.
37. Kim, S.W., et al., *Outer membrane vesicles from β-lactam-resistant Escherichia coli enable the survival of β-lactam-susceptible E. coli in the presence of β-lactam antibiotics.* Scientific Reports, 2018. **8**(1): p. 5402.
38. Schwechheimer, C., D.L. Rodriguez, and M.J. Kuehn, *NlpI-mediated modulation of outer membrane vesicle production through peptidoglycan dynamics in Escherichia coli.* MicrobiologyOpen, 2015. **4**(3): p. 375-389.
39. Manning, A.J. and M.J. Kuehn, *Contribution of bacterial outer membrane vesicles to innate bacterial defense.* BMC Microbiology, 2011. **11**(1): p. 258.
40. Kim, S.W., et al., *The Importance of Porins and β-Lactamase in Outer Membrane Vesicles on the Hydrolysis of β-Lactam Antibiotics.* International Journal of Molecular Sciences, 2020. **21**(8): p. 2822.